An investigation of non-equilibrium heat transport in a gas system under external force field

Tianbai Xiao [a], Kun Xu [b,c,*], Qingdong Cai [a], Tiezheng Qian [b]

[a] *Department of Mechanics and Engineering Science, College of Engineering, Peking University, Beijing 100871, China*
[b] *Department of Mathematics, Hong Kong University of Science and Technology, Clear Water Bay, Kowloon, Hong Kong*
[c] *Department of Mechanical and Aerospace Engineering, Hong Kong University of Science and Technology, Clear Water Bay, Kowloon, Hong Kong*

ARTICLE INFO

ABSTRACT

The gas dynamics under external force field is essentially associated with multiple scale nature due to the large variations of density and local Knudsen number. Single scale governing equations, such as the Boltzmann and Navier-Stokes equations, are valid in their respective modeling scales. Without identifying a physical scale between the above two limits for the modeling of the flow motion, it is challenging to develop a multiple scale method to capture non-equilibrium flow physics seamlessly across all regimes. Based on the modeling scale of cell size and implementing conservation laws directly in a discretized space, a well-balanced unified gas-kinetic scheme (UGKS) for multiscale gaseous flow has been constructed and used in the study of non-equilibrium flow and heat transport under external force field. In this paper, static heat conduction problems under external force field in different flow regimes are quantitatively investigated. In the lid-driven cavity case, the stratified flow is observed under external force field. With the increment of external force, the flow topological structure changes dramatically, and the temperature gradient, shearing stress, and external force play different roles in the determination of the total heat flux in different layers corresponding to different flow regimes. As a typical non-Fourier's heat conduction phenomena in the transition regime, the external force enhances the heat flux significantly along the forcing direction, with the relationship $\vec{q}_{force} \propto \vec{\phi}$, where $\vec{q}_{force}$ is the force-induced heat flux and $\vec{\phi}$ is the external force acceleration. This relationship is valid in all flow regimes with non-vanishing viscosity coefficient or the limited length of particle mean free path. Both theoretical analysis and numerical experiments are used to show the important role of external force on non-equilibrium heat transfer.

© 2018 Elsevier Ltd. All rights reserved.

1. Introduction

The gas dynamics under external force field is usually associated with multiple scale nature due to the possible large variation of gas density and local Knudsen number along the direction of force. On mesoscopic level, the kinetic theory could be employed to illustrate the physical effect of external force. In the kinetic scale, the Boltzmann equation follows the evolution of velocity distribution function $f(x_i, t, u_i)$ to describe the particle transport and collision assembly. With an external forcing acceleration ϕ_i acting on the particles, the evolving process of f is modeled in Eq. (1) with separate operators: the free flight of the particles (left hand terms) and their collisions (right hand term), i.e.,

$$\frac{\partial f}{\partial t} + u_i \frac{\partial f}{\partial x_i} + \phi_i \frac{\partial f}{\partial u_i} = Q(f). \tag{1}$$

Here u_i is the particle velocity and $Q(f)$ is the collision term. For a real gas dynamic system, even with an initial Maxwellian of a barometric distribution under external force, the free transport of particles between two successive collisions always evolves the system towards to a non-equilibrium state. Under external force field, the particle acceleration or deceleration process during this time interval results in a distortion of the distribution function in the velocity space. The deviation from equilibrium distribution is restricted by the particle collision time τ. On the other hand, the particle collision takes effect to push the system back towards equilibrium state. In continuum flow, the deviation from equilibrium is weak due to intensive intermolecular collisions, and thus the non-equilibrium transport is well described with viscosity and heat conductivity in the constitutive relationship. However, in transition and rarefied regime, the particle free transport and collision are loosely coupled

due to a large particle collision time. Much complicated nonlinear dynamics due to external force on the movement of particles between collisions can emerge and present a peculiar non-conventional energy or heat conduction transport phenomena. The strong non-equilibrium effects are expected in an even highly dissipative regions, such as the shock and boundary layers. To investigate the heat conduction problem under the existence of external force field is important to understand the dissipative flow physics.

It is noted that there is only limited study on non-equilibrium flow under external force field [1,2]. Generally, the existence of external force field, such as gravity, introduces a characteristic length scale $H \sim k_B T/m\phi$ [3], where k_B is the Boltzmann constant, m is the particle mass and ϕ is the magnitude of external forcing acceleration. It denotes a length scale over which the force field produces a significant effect on the gas evolution. For a gravitational system on the Earth atmosphere H is of $O(10^3)$ meters, and under laboratory condition or a micro-electro-mechanical system (MEMS) with geometric characteristic length L, the relation $H \gg L$ holds naturally, and thus it is reasonable to omit the influence of external force effect. However, in the case where H is comparable to L, the effect of external force will appear. For a large-scale system in stellar and planetary atmosphere, the force will result in significant change of gas density, and so is the variation of the particle mean free path and the local Knudsen number. Similar cases may appear in small scale, but with large acceleration, such as material interface with shock impingement. It is interesting to study the multiple scale non-equilibrium transport under external force filed.

The current existing governing equations for the gas dynamics, such as the Boltzmann and Navier-Stokes, are constructed on their respective modeling scales. For example, the Boltzmann equation is defined on the particle mean free path and collision time. Only on such a modeling scale, the particle transport and collision can be separately formulated, and the solutions in other scales by applying the Boltzmann equation is mainly due to accumulation of flow dynamics in the mean free path and particle collision time scale. The Navier-Stokes-Fourier (NSF) equations are constructed to describe fluid motion and heat transfer on a macroscopic level with limited number of flow variables. The fluid element is the finest closed unit in the NS modeling, where intensive particle collisions prevent particle penetration between adjacent fluid elements. The successful applications of the NS and Boltzmann equations are on their valid scales with a clear scale separation. However, for a system under external force field, the flow physics may vary continuously from the kinetic Boltzmann modeling in the upper rarefied layer to the hydrodynamic one in the lower dense region. The continuous variation of characteristic scale length should associate with a continuum spectrum of gas dynamics to connect the Boltzmann and NS seamlessly. However, it is challenging to construct such a multiple scale governing equation with flexible degrees of freedom to describe a scale-dependent dynamics, such as a general equation to in all scales from kinetic to hydrodynamic ones. The mathematical derivation of extended hydrodynamic equations will not be very successful if a modeling scale is not specifically pointed out. Unfortunately, there is no a clear physical scale for modeling between the Boltzmann and NS limits.

For conventional research of gas dynamics, the modeling and computation are handled separately. Once the governing equations are given, the CFD method serves to get numerical solution of differential equations, such as direct Boltzmann solver [4] for the Boltzmann equation and Riemann solver [5] for macroscopic fluid dynamic equations. Without valid multiple scale governing equations, the traditional CFD can be hardly used for solving multiple scale flow problem. In order to construct a multiscale method,

the physics modeling is directly used in the construction of a numerical algorithm. Based on the cell size and time step scales, the corresponding discretized multiscale governing equations have been constructed in the well-balanced unified gas-kinetic scheme (UGKS) for flow problem under external force field [6–8]. Through a coupled treatment of particle transport, collision, and external forcing effect in the mesh size scale for the flux transport across a cell interface, a cross-scale flow physics from kinetic particle transport to hydrodynamic wave propagation has been incorporated in the scheme [9]. In the current work, the well-balanced UGKS will be employed to investigate the non-equilibrium gas evolution under external force field.

In this paper, the heat transfer in the lid-driven cavity flow is used as a typical example for the study of non-equilibrium gas dynamics under external force field with a large variation of gas density. Even under such a simple geometry, the cavity flow displays complicated flow phenomena with multiple scale transport, including shearing layers, eddies, secondary flows, heat transfer, hydrodynamic instabilities, and laminar-turbulence transition, etc [10]. Great efforts have been devoted to the study of the flow physics in different flow regimes. In the continuum regime, the cavity problem is a typical benchmark case for the validation of numerical algorithms for the NS solutions [10–15]. In rarefied regime, the direct simulation Monte Carlo (DSMC) [16] and Boltzmann solvers [17,18] provide the benchmark solutions. Naris et al. [19] discretized a linearized BGK equation to investigate the rarefaction effect on the flow pattern and dynamics over the whole range of the Knudsen number. Mizzi et al. [20] compared the simulation results from the Navier-Stokes-Fourier equations (NSF) with slip boundary conditions and the DSMC results in a lid-driven micro cavity case. John et al. [21] applied the DSMC, discovered counter-gradient heat transport in the transition regime, and investigated the dynamic effect from the expansion cooling and viscous heating on the heat transport mechanism. In all previous work, there is few study about the flow under external force field. Due to the external force effect, the cavity flow becomes even more complicated with its non-equilibrium multiple scale evolution. A few new phenomena, including the connection between the heat transfer and external force, and stratified flow of different regimes, have been observed through this study.

This paper is organized as follows. The basic kinetic theory and the analysis of external force on a gas dynamic system are presented in Section 2. Section 3 presents the numerical experiment and discussion on the non-equilibrium flow and heat transfer across different flow regimes. The last section is the conclusion.

2. Analysis on physical effect from external force

In the Chapman-Enskog expansion [22], the particle distribution function is expanded into series around the equilibrium state with respect to a small factor ϵ,

$$f = f^{(0)} + f^{(1)}\epsilon + f^{(2)}\epsilon^2 + \cdots, \tag{2}$$

and different truncations correspond to different fluid dynamic equations. With zeroth-order approximation, the distribution function stays in the exact Maxwellian, and the vanishing contribution of collision operator $Q(f)$ in Eq. (1) leads to the Euler equations [23],

$$\frac{\partial \rho}{\partial t} + \frac{\partial}{\partial x_i}(\rho U_i) = 0,$$

$$\frac{\partial}{\partial t}(\rho U_i) + \frac{\partial}{\partial x_j}(\rho U_i U_j + p\delta_{ij}) = -\rho \phi_i,$$

$$\frac{\partial}{\partial t}\left[\rho\left(e + \frac{1}{2}U_i U_i\right)\right] + \frac{\partial}{\partial x_j}\left[\rho U_j\left(e + \frac{1}{2}U_i U_i\right) + U_i p\delta_{ij}\right] = -\rho U_j \phi_j.$$

$$\tag{3}$$

The notation δ_{ij} is Kronecker's delta, e is the internal energy and ϕ_i is the external forcing acceleration.

Due to the complexity of the Boltzmann collision operator, here we will use the BGK equation [24] to qualitatively demonstrate the asymptotic expansion under external force field. In the BGK equation, the collision operator is replaced by a relaxation term, i.e.,

$$\frac{\partial f}{\partial t} + u_i \frac{\partial f}{\partial x_i} + \phi_i \frac{\partial f}{\partial u_i} = \frac{f^+ - f}{\tau}. \tag{4}$$

Here $\tau = \mu/p$ is the collision time, where μ is viscosity coefficient and p is pressure. The Maxwellian distribution f^+ for a monatomic gas is

$$f^+ = \rho \left(\frac{\lambda}{\pi}\right)^{\frac{3}{2}} e^{-\lambda[(u_i - U_i)^2]}, \tag{5}$$

where $\lambda = m/2k_B T$ with m the particle mass, k_B the Boltzmann constant. In the near-equilibrium region, the expansion in Eq. (2) is carried out with respect to the particle collision time or its corresponding Knudsen number, which can be written into the following successive form [25],

$$f = f^+ - \tau \frac{D}{Dt} f^+ + \tau \frac{D}{Dt}\left(\tau \frac{D}{Dt} f^+\right) + \cdots, \tag{6}$$

where D/Dt is the total derivative of both physical and velocity space. For the first order truncation of Eq. (6) to the collision time τ, the distribution function f has the corresponding expansion form,

$$f = f^+ - \tau(f_t^+ + u_i f_{x_i}^+ + \phi_i f_{u_i}^+) + O(\tau^2). \tag{7}$$

The above derivatives in physical and velocity space can be obtained by the chain rule from the Maxwellian distribution in Eq. (5), i.e.,

$$\frac{\partial f^+}{\partial t} = \frac{1}{\rho} \frac{\partial \rho}{\partial t} f^+ + \frac{3}{2\lambda} \frac{\partial \lambda}{\partial t} f^+ + \left(-u_i^2 + 2u_i U_i - U_i^2\right) \frac{\partial \lambda}{\partial t} f^+$$
$$+ (2u_i \lambda - 2U_i \lambda) \frac{\partial U_i}{\partial t} f^+,$$

$$\frac{\partial f^+}{\partial x_i} = \frac{1}{\rho} \frac{\partial \rho}{\partial x_i} f^+ + \frac{3}{2\lambda} \frac{\partial \lambda}{\partial x_i} f^+ + \left(-u_j^2 + 2u_j U_j - U_j^2\right) \frac{\partial \lambda}{\partial x_i} f^+$$
$$+ (2u_j \lambda - 2U_j \lambda) \frac{\partial U_j}{\partial x_i} f^+,$$

$$\frac{\partial f^+}{\partial u_i} = -2\lambda(u_i - U_i) f^+,$$

and the time derivatives are replaced by the spatial ones from the following Euler equations,

$$\frac{\partial \rho}{\partial t} = -\frac{\partial \rho U_i}{\partial x_i},$$
$$\frac{\partial U_i}{\partial t} = -U_j \frac{\partial U_i}{\partial x_j} - \frac{1}{\rho} \frac{\partial p}{\partial x_i} + \phi_i,$$
$$\frac{\partial T}{\partial t} = -U_i \frac{\partial T}{\partial x_i} - \frac{2}{3} \frac{\partial U_i}{\partial x_j}, \tag{8}$$
$$\frac{\partial \lambda}{\partial t} = U_i \frac{\partial \lambda}{\partial x_i} - \frac{4k_B \lambda^2}{3m} \frac{\partial U_i}{\partial x_j}.$$

Substituting the expanded distribution function into the original BGK equation and take conservative moments over velocity space, the corresponding Navier-Stokes equations can be obtained,

$$\frac{\partial \rho}{\partial t} + \frac{\partial}{\partial x_i}(\rho U_i) = 0,$$
$$\frac{\partial}{\partial t}(\rho U_i) + \frac{\partial}{\partial x_j}(\rho U_i U_j + P_{ij}) = -\rho \phi_i,$$
$$\frac{\partial}{\partial t}\left[\rho\left(e + \frac{1}{2}U_i U_i\right)\right] + \frac{\partial}{\partial x_j}\left[\rho U_j\left(e + \frac{1}{2}U_i U_i\right) + U_i P_{ij} + q_j\right] = -\rho U_j \phi_j. \tag{9}$$

The stress tensor P_{ij} and heat flux q_i are related to the non-vanishing effect of particle collision time in the kinetic scale [26], i.e.,

$$P_{ij} = p\delta_{ij} - \mu\left(\frac{\partial U_i}{\partial x_j} + \frac{\partial U_j}{\partial x_i} - \frac{2}{3} \frac{\partial U_k}{\partial x_k} \delta_{ij}\right), \quad q_i = -\kappa \frac{\partial T}{\partial x_i},$$

where μ and κ are the viscosity and thermal conductivity coefficients, which are proportional to τ.

In the above Chapman-Enskog framework, the macroscopic flow dynamics and heat transfer are connected to the particle motion at kinetic level. In the first-order Euler Eqs. (8), only velocity is affected by external force field, and there are no contributions to the thermodynamic variables, such as density and temperature. In the steady Euler limit under a conservative force potential Φ, where the potential is independent of time and molecular velocity, the corresponding kinetic equation goes to

$$u_i \frac{\partial f}{\partial x_i} - \frac{\partial \Phi}{\partial x_i} \frac{\partial f}{\partial u_i} = 0. \tag{10}$$

The general solution of Eq. (10) is

$$f(x_i, u_i) = \mathcal{F}\left(\Phi + \frac{1}{2} u_i u_i\right),$$

where $\mathcal{F}$ is an arbitrary function. In this solution, the temperature becomes a constant multiplier for the function of $(\Phi + \frac{1}{2} u_i u_i)$ [27,28], and it shows an isothermal hydrostatic equilibrium flow, which is also a solution of Eq. (3),

$$\rho = \rho(x_i), \quad U = 0, \quad \frac{\partial p}{\partial x_i} = -\rho \frac{\partial \Phi}{\partial x_i}.$$

For a constant gravitational acceleration $\phi_i = -\partial \Phi/\partial x_i$, the corresponding solution is,

$$\rho = \rho_0 \exp\left(\frac{\phi_i x_i}{RT}\right), \quad u = 0, \quad p = p_0 \exp\left(\frac{\phi_i x_i}{RT}\right), \tag{11}$$

where R is the gas constant. Since there is no macroscopic velocity or its derivatives involved, the Euler and Navier-Stokes equations will follow the same steady state solution in Eq. (11).

However, for the non-equilibrium gas dynamics with non-vanishing particle mean free path and collision time, the distribution function under external force field will not rigorously follow the Chapman-Enskog form in Eq. (7). This problem can be qualitatively illustrated by the kinetic model. As shown in Fig. 1, a column of gas is enclosed between two parallel plates. The upper and lower plates are kept with the constant temperatures T_u and T_d. The gas is static everywhere with no macroscopic flow. With a virtual interface I inside the domain, the following thought experiment can be carried out to illustrate the effect of external force on the gas transport with limited particle mean free path. Let's consider the molecules transport across an imaginary interface I in the middle of the domain. A group of molecules transporting downwards are denoted as A, which are located within a particle mean free path ℓ_A above the interface. Similarly, a group of upward moving particles are named B with ℓ_B below the interface, see Fig. 1. The steady state under the condition $T_d > T_u$ without external force field is a diffusion problem with uniform pressure and without macroscopic flow velocity. As a result, the density increases and temperature decreases in the positive x direction. Therefore, across the interface I there are more molecules with lower mean velocity coming from the point A, and less molecules with higher speed from the point B. The requirement of zero net particle flux transport across the interface is satisfied, and the steady state is remained. For the energy flux at I, the molecules from B carry more energy than those from A because the energy flux is related to the higher-order moments of particle velocity, such as to the order c^3. Thus, a steady state in this case is associated with the heat flux in
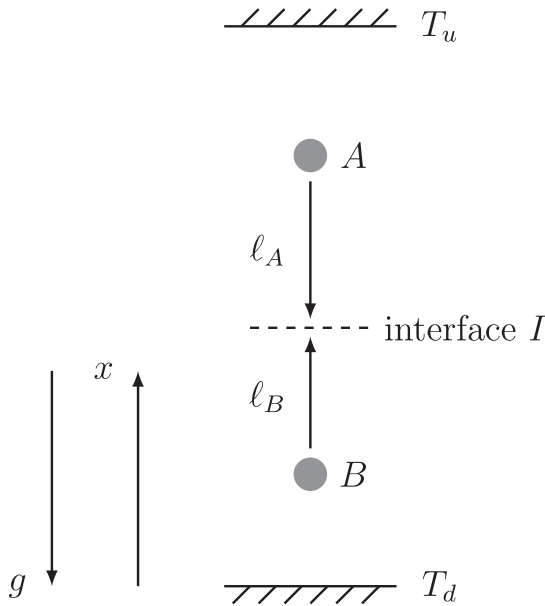
Fig. 1. Schematic of gas enclosed between two plates.

the upward direction, which follows the Fourier's law. Now, let us suddenly add a constant external force field along the negative x-direction $\phi_x = -\Phi_x = -g$ into the above heat conduction system. Under external force field, from the point A/B to the interface I, the particles from A (B) will get accelerated (decelerated) in a mean free path length, resulting in $c'_A > c_A$ and $c'_B < c_B$. Therefore, the original upward heat flux will be suppressed. When the magnitude of external force is small, the effect of force field performs a small modification above the previous heat flux. However, if the force is relative large, it may even play the dominant role over the Fourier-type thermal conduction in the heat flux. Complicated energy transport will happen under strong external field with an even large particle mean free path in the non-equilibrium regime. Analogously, if the direction of force ϕ_x is changed into positive x-direction, aligned with the original heat flux, the particle velocity changes $c'_A < c_A$ and $c'_B > c_B$ will enhance the heat flux accordingly.

The above analysis on the mechanism of particle and energy transport under external force field is on the particle free transport mechanism within a particle mean free path scale. This physical effect appears in all flow regimes with non-vanishing particle mean free path and collision time. In the NS regime, the viscosity and heat conductivity coefficients correspond to non-vanishing particle mean free path in the relationship $\mu, \kappa \propto \rho c \ell$, where ρ is the density, c is the mean particle velocity, and ℓ is the particle mean free path [27], and the heat transport contribution from the external force will appear definitely, especially under non-equilibrium unsteady condition. The above picture can be demonstrated as well using kinetic differential equation. For brevity, let us consider one dimensional case first, i.e.,

$$\frac{Df}{Dt} = \frac{\partial f}{\partial t} + u \frac{\partial f}{\partial x} + \phi_x \frac{\partial f}{\partial u} = \frac{f^+ - f}{\tau},$$

and the corresponding Maxwellian distribution f^+ is

$$f^+ = \rho \left(\frac{\lambda}{\pi}\right)^{\frac{K+1}{2}} e^{-\lambda \left[(u-U)^2 + \xi^2\right]}, \tag{12}$$

where K is the degree of freedom for the internal motion ξ. For a monatomic gas in one dimensional flow, it sets $K = 2$ to account for the random motions in y and z directions. Within a small time interval, it is reasonable to regard the collision time τ as a local

constant, then the BGK equation has the following evolving solution from arbitrary initial state at (x^0, t^0, u^0), i.e.,

$$f(x, t, u, \xi) = \frac{1}{\tau} \int_{t^0}^t f^+(x', t', u', \xi) e^{-(t-t')/\tau} dt' + e^{-(t-t^0)/\tau} f_0(x^0, t^0, u^0, \xi), \tag{13}$$

where $x' = x - u'(t - t') - \frac{1}{2}\phi_x(t - t')^2, u' = u - \phi_x(t - t')$ are the particle trajectories in physical and velocity space, and $(x^0, u^0) = (x - (u - \phi_x t)t - \frac{1}{2}\phi_x t^2, u - \phi_x t)$ is the initial location for the particle in phase space which passes through the cell interface at time $x = 0, t$. For simplicity, we rewrite the position (x, t^0) as $(0, 0)$, and the corresponding solution becomes

$$f(0, t, u, \xi) = \frac{1}{\tau} \int_0^t f^+(x', t', u', \xi) e^{-(t-t')/\tau} dt' + e^{-t/\tau} f_0(-(u - \phi_x t)t - \frac{1}{2}\phi_x t^2, 0, u - \phi_x t, \xi) = \tilde{f}^+ + \tilde{f}_0. \tag{14}$$

The first term $\tilde{f}$ is from the integral of equilibrium distribution along the characteristic line. In addition, the latter term $\tilde{f}_0$ recovers particle free transport from the initial distribution function f_0. With the Taylor expansion, to the first order of evolving time t, we have

$$\tilde{f}_0 = e^{-t/\tau} \left[f_0(0, 0, u, \xi) - \frac{\partial f_0}{\partial x} ut - \frac{\partial f_0}{\partial u} \phi_x t \right] + O(t^2). \tag{15}$$

In the above solution, the spatial slope related terms describe the free transport of particles in physical space due to the inhomogeneous spatial field. At the same time, the force acceleration distorts the distribution function in the velocity space with the contributions of the last term.

As macroscopic variables are related with particle distribution function through velocity moments,

$$\mathbf{W} = \begin{pmatrix} \rho \\ \rho U \\ \rho E \end{pmatrix} = \int \psi f d\Xi,$$

$$p = \frac{1}{3} \int \left((u - U)^2 + \xi^2\right) f d\Xi,$$

$$q = \frac{1}{2} \int (u - U)\left((u - U)^2 + \xi^2\right) f d\Xi,$$

where $d\Xi = dud\xi, p$ is pressure, q is heat flux and $\psi = (1, u, \frac{1}{2}(u^2 + \xi^2))^T$ is the vector of moments for collision invariants. They give the contributions from the solution (15) to the macroscopic flow transport. As shown in the expression of $\tilde{f}_0$ in Eq. (15), the detailed form of distribution function depends on the initial flow condition. As a simple homogeneous case, the spatial derivatives can be assumed to be absent for simplicity. The initial particle distribution function f_0 is set as the Maxwellian f^+, and thus its velocity moments $\int u^\alpha \xi^\beta f^+ d\Xi = \rho\langle u^\alpha \xi^\beta \rangle$ has the property that

$$\langle u^\alpha \xi^\beta \rangle = \langle u^\alpha \rangle \langle \xi^\beta \rangle,$$

where the moments of Gaussian distribution can be evaluated through [29],

$$\langle u^0 \rangle = 1,$$
$$\langle u^1 \rangle = U,$$
$$\cdots,$$
$$\langle u^{n+2} \rangle = U\langle u^{n+1} \rangle + \frac{n+1}{2\lambda} \langle u^n \rangle,$$
$$\langle \xi^2 \rangle = \frac{K}{2\lambda},$$

where n is an integer. Since there is no contribution from spatial derivatives here, the net contribution of macroscopic transport from the external force can be evaluated as

$$\Delta \mathbf{W} = \begin{pmatrix} \Delta \rho \\ \Delta \rho U \\ \Delta \rho E \end{pmatrix} = e^{-t/\tau} \int \psi (-t\phi_x f_u^+) d\Xi,$$

$$\Delta p = \frac{e^{-t/\tau}}{3} \int \left((u-U)^2 + \xi^2 \right)(-t\phi_x f_u^+) d\Xi,$$

$$\Delta q = \frac{e^{-t/\tau}}{2} \int (u-U)\left((u-U)^2 + \xi^2 \right)(-t\phi_x f_u^+) d\Xi.$$

If the forcing term ϕ_x and the evolving time t are viewed as local constants, after integration by parts, we have the following relations,

$$\Delta \mathbf{W} = \begin{pmatrix} \Delta \rho \\ \Delta \rho U \\ \Delta \rho E \end{pmatrix} = e^{-t/\tau} t\phi_x \rho \begin{pmatrix} 0 \\ 1 \\ U \end{pmatrix}, \tag{16}$$

$$\Delta p = \frac{e^{-t/\tau}}{3} t\phi_x \rho \left(2\langle u^1 \rangle - 2U\langle u^0 \rangle \right) = 0, \tag{17}$$

$$\Delta q = \frac{e^{-t/\tau}}{2} \tau \phi_x \rho \left(3\langle u^2 \rangle - 6U\langle u \rangle + 3U^2\langle u^0 \rangle \right) = \frac{(K+3)e^{-t/\tau}}{4} \frac{t\phi_x \rho}{\lambda}. \tag{18}$$

The Eqs. (16)–(18) present qualitative contributions from external force field on the macroscopic flow evolution. The contribution in macroscopic equations is exactly due to the external force effect during the particle free transport between two successive collisions. The isotropic pressure is not affected by the external field in the current order of Taylor expansion. However, it is clear that there exists contribution to the heat flux from the external forcing term under current order of expansion. The heat flux along the positive direction of external force acceleration ϕ_x has been enhanced. In other words, the external force will contribute the heat flux transport in the forcing direction.

The above analysis is consistent with the one in [3], where a first-order modification on the heat flux from gravity is illustrated using asymptotic perturbation method. A limited particle collision time τ corresponds to a non-vanishing viscosity and heat conduction coefficients. Therefore, on the Navier-Stokes order the external forcing term will affect the heat energy transport, especially in unsteady non-equilibrium regimes. It is noted that the above analysis is for the case of small time interval and small external force under a homogeneous initial condition. With the increment of external force and degree of rarefaction, non-equilibrium transport phenomena are expected to appear. Fortunately, we have designed an accurate multiscale method [8], which can be used to study the non-equilibrium heat transport under external force field in all flow regimes.

3. Non-equilibrium flow studies

In this section, we are going to present and discuss several numerical experiments to investigate the non-equilibrium flow dynamics under external force field. The well-balanced unified gas-kinetic scheme (UGKS) is employed in all cases [8].

3.1. Poiseuille-type flow

In the first numerical experiment, we investigate the steady flow of dilute gas between two infinite parallel plates driven by a unidirectional external force [30–36]. This case serves as a supplementary validation of the current numerical algorithm besides the cases presented in Ref. [8]. The two plates at rest are located at $y = \pm L/2$ and kept at temperature T_0. The gas at rest initially has a uniform density ρ_0 and temperature T_0, and subject to a uniform external force in the positive x direction, i.e., in the direction parallel to the plates. The initial particle distribution function is set as the Maxwellian everywhere in the flow domain. There is no pressure gradient in the x direction. If we consider this problem in the framework of the Navier-Stokes equations, then it is a simple one-dimensional example. In the framework of kinetic theory, the steady BGK model equation for Maxwell molecules under external force field is used to describe the gas evolution in this system,

$$v\frac{\partial f}{\partial y} + \phi_x \frac{\partial f}{\partial u} = A_c \rho (f^+ - f), \tag{19}$$

where A_c is a constant and the collision frequency is $1/\tau = A_c \rho$. The Maxwellian diffusive reflection boundary is assumed in the simulation.

With the dimensionless variables defined as

$$\hat{x} = \frac{x}{L_0}, \quad \hat{y} = \frac{y}{L_0}, \quad \hat{\rho} = \frac{\rho}{\rho_0}, \quad \hat{T} = \frac{T}{T_0},$$

$$\hat{u}_i = \frac{u_i}{(2RT_0)^{1/2}}, \quad \hat{U}_i = \frac{U_i}{(2RT_0)^{1/2}}, \quad \hat{f} = \frac{f}{\rho_0(2RT_0)^{3/2}},$$

$$\hat{P}_{ij} = \frac{P_{ij}}{\rho_0(2RT_0)}, \quad \hat{q}_i = \frac{q_i}{\rho_0(2RT_0)^{3/2}}, \quad \hat{\phi}_i = \frac{\phi_i}{2RT_0/L_0},$$

where u_i is the particle velocity, U_i is the macroscopic flow velocity, P_{ij} is the stress tensor, q_i is the heat flux and ϕ_i is the external force acceleration, the dimensionless BGK equation writes

$$\hat{v}\frac{\partial \hat{f}}{\partial \hat{y}} + \hat{\phi}_x \frac{\partial \hat{f}}{\partial \hat{u}} = \frac{2}{\sqrt{\pi}} \frac{1}{Kn} \hat{\rho}(\hat{f}^+ - \hat{f}),$$

where Kn is the Knudsen number in the reference state. The collision constant is absorbed with unit value $A_c = 1$. For simplicity, we will drop the hat notation henceforth to denote dimensionless variables.

To describe this basic system, Aoki and his co-workers used the asymptotic analysis [33] for small Knudsen numbers and derived a system of fluid-dynamic-type equations and their boundary conditions up to the second order. The Hilbert expansion and its Knudsen layer correction are carried out with respect to $\epsilon = (\sqrt{2}/\pi)Kn$, and the external force acceleration is set as $\phi_x = \alpha Kn$. At large Knudsen number, the asymptotic theory fails. A number of numerical experiments have been conducted by means of a finite difference method to solve the BGK equation Eq. (19) at different Kn and α in [33]. In the following, we use the well-balanced UGKS with 100 uniform physical cells in $[-0.5, 0.5]$ and 41 uniform velocity points in $[-5, 5]$, to simulate the cases with $Kn = 0.02, 0.05, 0.1$ and $\alpha = 1, 2, 3$, and compare the UGKS results with the asymptotic solutions and the finite difference ones [33].

Figs. 2–4 show the profiles of the density, U-velocity and temperature for $\alpha = 1$, 2, and 3 in the upper half ($0 \leqslant Y \leq 0.5$) of the flow domain. Figs. 5–7 are the results of the stress tensor components P_{xx}, P_{xy} and P_{yy} of the stress tensor and the heat fluxes q_x and q_y. The lines (solid, dashed and dash dot) are the results calculated by the well-balanced UGKS, the circles indicate asymptotic solutions, and the deltas denote the reference results by Aoki's finite difference method. It can be seen that in the cases with low Knudsen number, the UGKS solutions correspond well with the asymptotic results. At $\alpha = 2$ and 3, there is a very small discrepancy between numerical solutions and asymptotic ones. The reason for such a deviation is that the asymptotic analysis is

confined up to the second order in the Knudsen number. When the Knudsen number and external force become relatively large, the high-order Hilbert expansion cannot reflect the physical reality. Therefore, in the cases with $Kn = 0.1$, the finite difference solutions (denoted by "FD result" in the figure) are supplemented as the benchmark results, which are consistent with the well-balanced UGKS solutions.

As reported in the previous research, an interesting non-equilibrium phenomenon in this force driven system is the bimodal temperature profile, with a hollow near the center between two plates. This effect was first pointed by Malek et al. [32] using the DSMC method, and reproduced by the kinetic simulation and theory [33–36]. The localized temperature profiles calculated by the UGKS and asymptotic solutions are presented in Fig. 8. In general, the temperature minimum in this case can be attributed to the contribution of higher order terms, and can be resolved with higher-order macroscopic equations, such as the super-Burnett one [34]. Although in Fig. 8 the second-order asymptotic analysis overestimates the strength of the temperature hollow, it is obvious that even for this simple case with rectangular geometry and uniform,
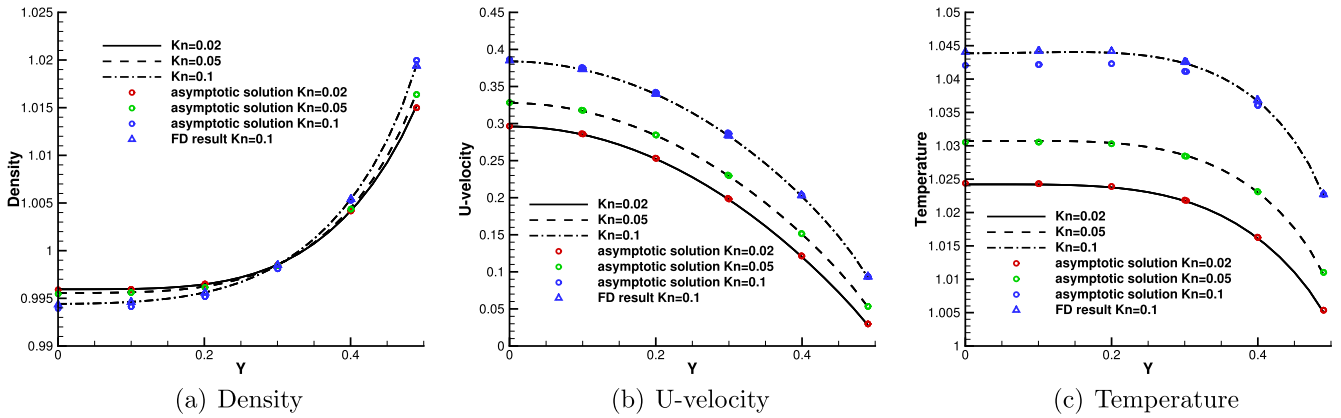

(a) Density   (b) U-velocity   (c) Temperature

Fig. 2. The profiles of density, U-velocity and temperature with $\alpha = 1$.

(a) Density   (b) U-velocity   (c) Temperature

Fig. 3. The profiles of density, U-velocity and temperature with $\alpha = 2$.
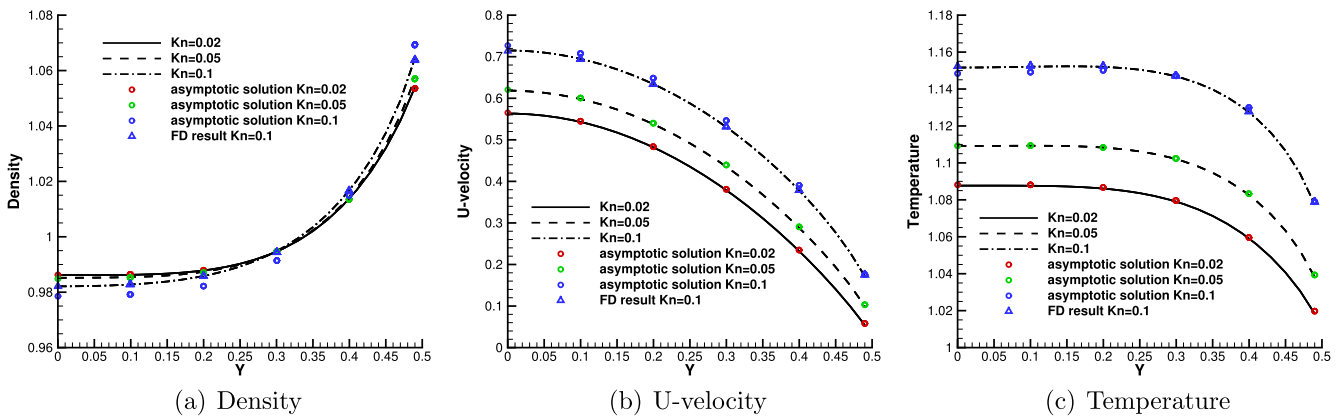

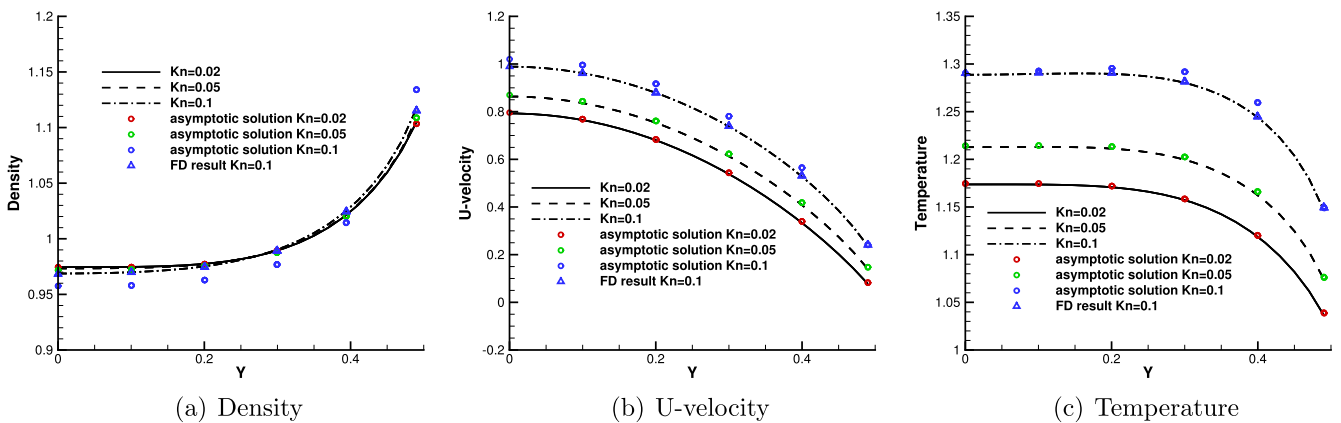(a) Density   (b) U-velocity   (c) Temperature

Fig. 4. The profiles of density, U-velocity and temperature with $\alpha = 3$.
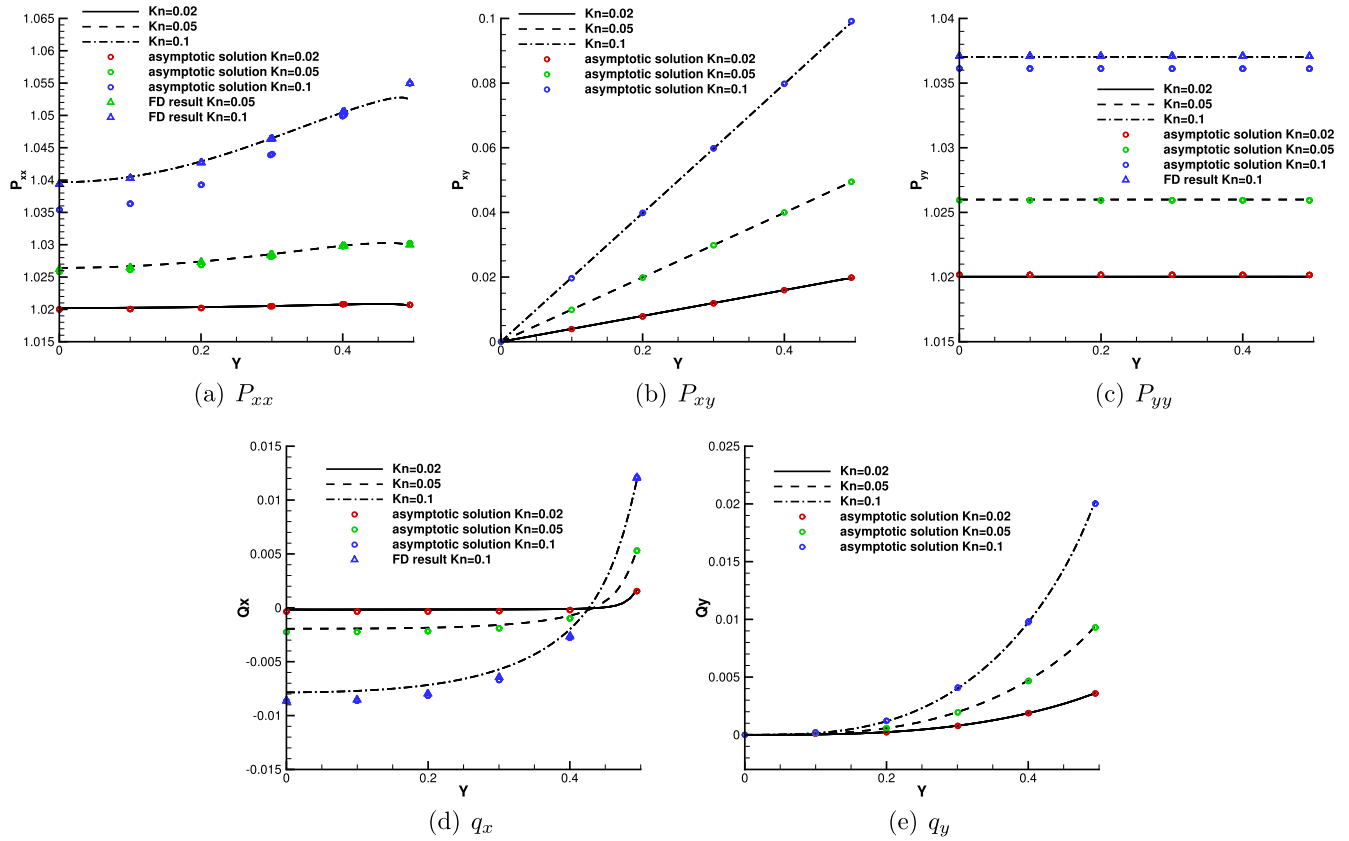
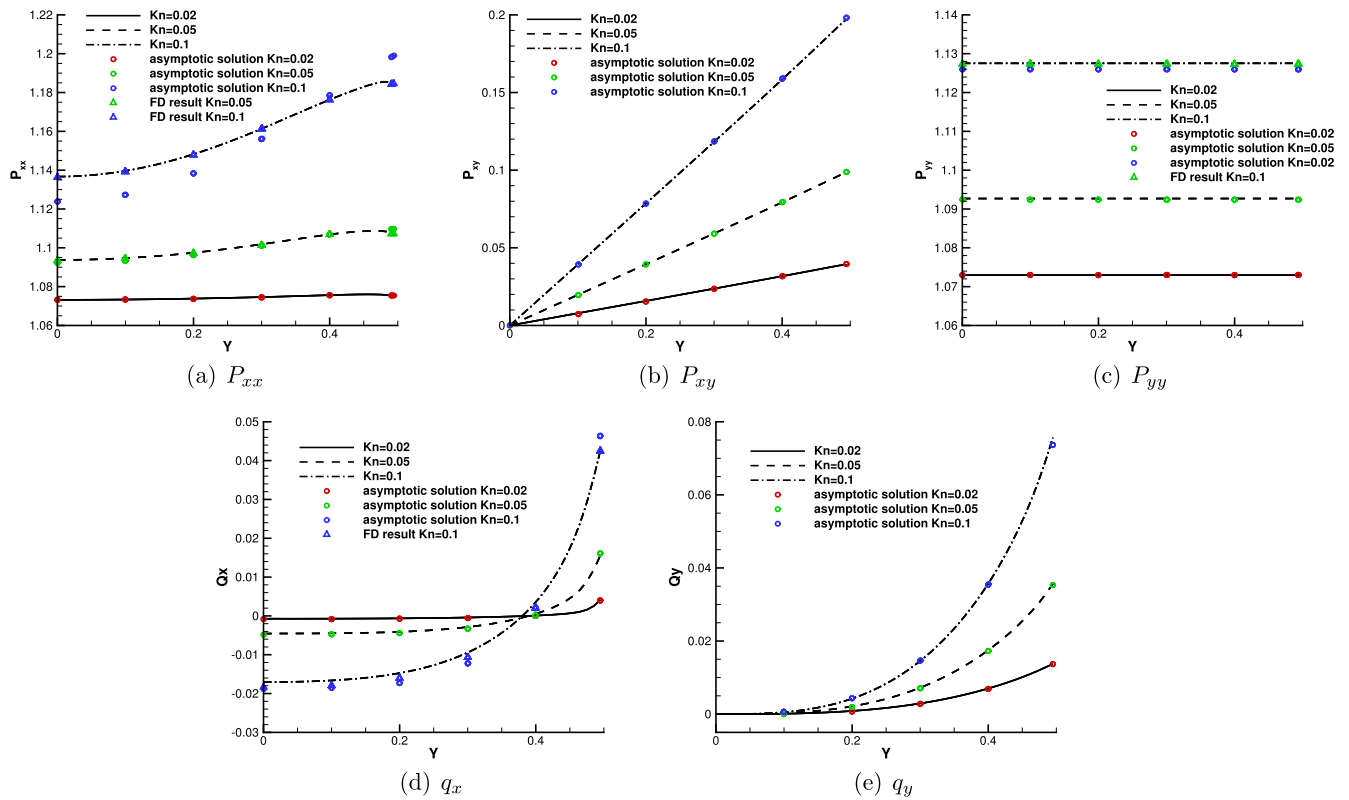**Fig. 5.** The profiles of stress and heat flux with $\alpha = 1$.

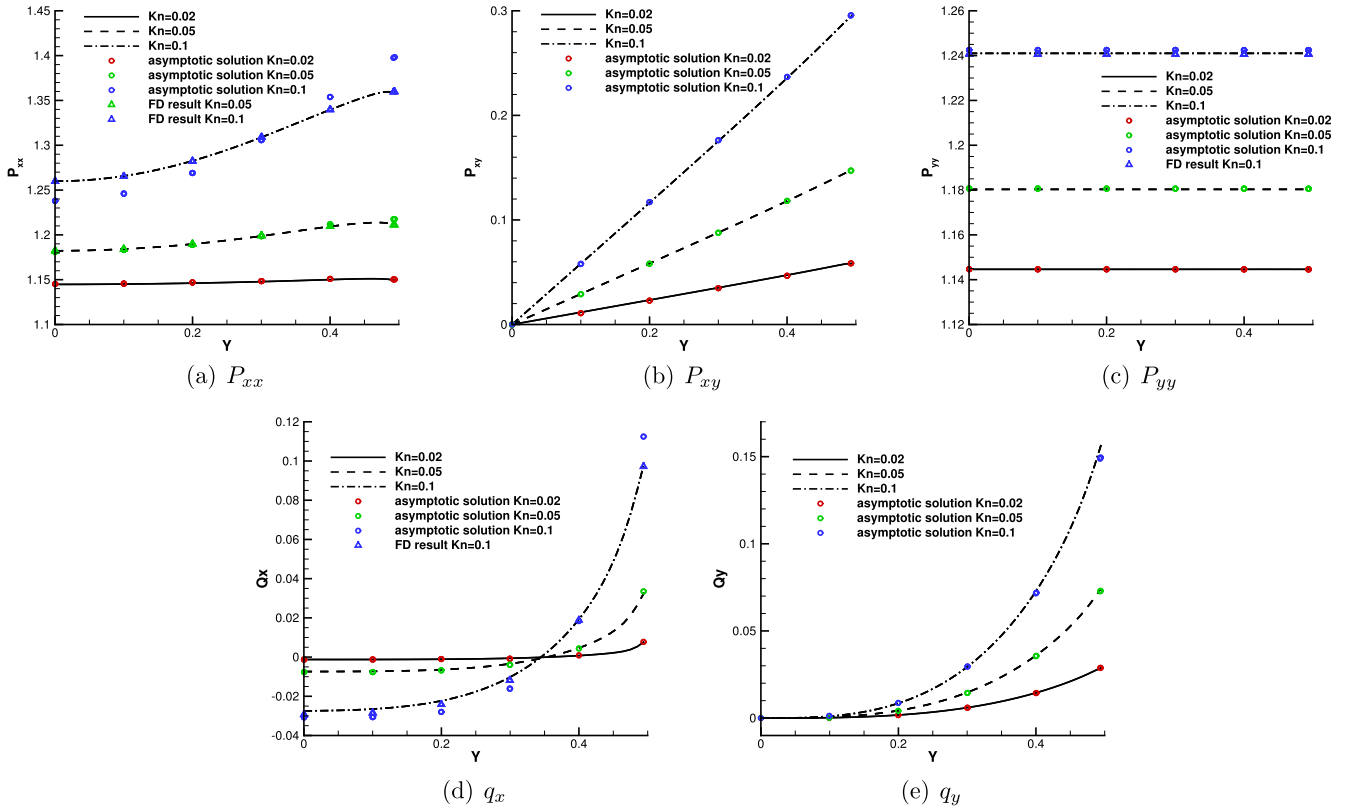**Fig. 6.** The profiles of stress and heat flux with $\alpha = 2$.

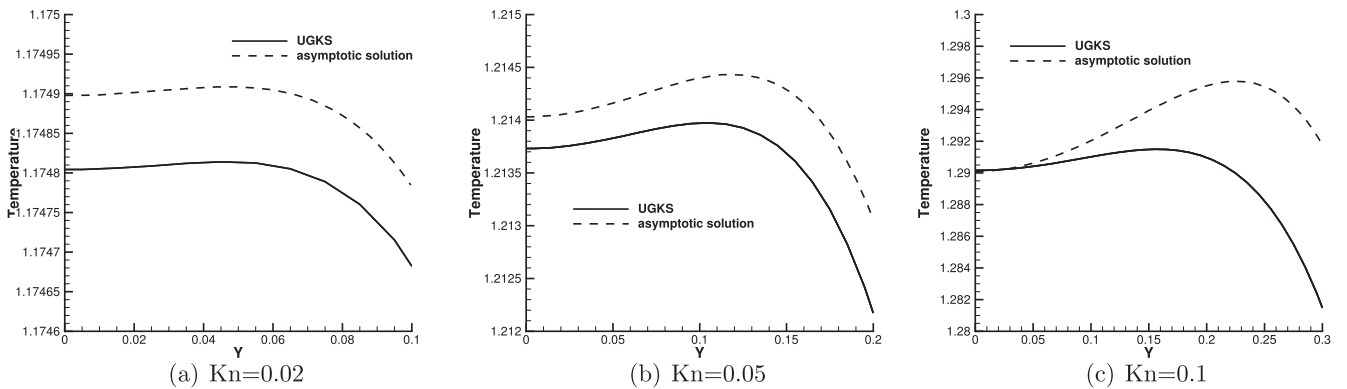**Fig. 7.** The profiles of stress and heat flux with $\alpha = 3$.

Fig. 8. The temperature profile in the central part with $\alpha = 3$.

weak external force, the Navier-Stokes equations fail to describe the accurate gas evolution. For non-equilibrium flow study, the use of kinetic modeling and computation becomes necessary. This case also validates the capacity of the well-balanced UGKS to simulate non-equilibrium gas dynamics under external force field.

3.2. Static heat conduction

Consider a column of gas enclosed between two infinite parallel plates at $x = 0$ and $x = 1$, both maintained with different temperature under a constant external force field perpendicular to the plates. Instead of studying the Rayleigh-Bénard convection [37,38], we study the static heat conduction problem and evaluate the contribution of heat flux due to the external force field. This is possible before the parameters approach to critical values, such that the Rayleigh number satisfies $Ra < Ra_c \simeq 1700$ in the incompressible limit.

Two ways can be used to describe the flow dynamics in this case. The one-dimensional Navier-Stokes-Fourier equations for this static system with the x-direction external force reduces to,

$$\frac{\partial}{\partial y} p = \rho \phi_x, \tag{20}$$

$$\frac{\partial}{\partial x}\left(\kappa(y)\frac{\partial}{\partial x}T\right) = 0, \tag{21}$$

where κ is the heat conductivity coefficient. At the same time, the steady one-dimensional BGK equation becomes

$$u\frac{\partial f}{\partial x} + \phi_x\frac{\partial f}{\partial u} = \frac{2}{\sqrt{\pi}}\frac{1}{Kn}\rho(f^+ - f), \tag{22}$$

where the collision frequency is $1/\tau = 2\rho/\sqrt{\pi}Kn$. Here all the flow variables are dimensionless unless special statements. As is

analyzed in Section 2, the external forcing term will influence the heat evolution process, resulting in a deviation of the profile away from the above theoretical solution given by Eq. (21).

We use the well-balanced UGKS with 100 uniform physical cells in $[0, 1]$ and 201 uniform velocity points in $[-5, 5]$ to simulate this case. The temperature ratio of the cold wall to the hot one is set to be $r = T_c/T_h = 0.9$. The initial uniform gas is at rest, with the same hot wall temperature. An external acceleration ϕ_x is imposed along the direction of temperature gradient to the system with different strengths $\phi_x = \pm 0.001, \pm 0.002, \pm 0.003, \pm 0.005, \pm 0.01, \pm 0.02, \pm 0.05, \pm 0.1, \pm 0.2, \pm 0.5, \pm 1.0$. Here the positive direction of external force is aligned with the direction of heat flux from wall temperature difference. Both temperature ratio and external force are set to be small to have static heat conduction solution.

As the net contribution from external force on heat flux is concerned, the solution at the middle point of the flow domain $x = 0.5$ is used for the analysis in order to minimize the effect from boundaries for the steady case in the absence of macroscopic flow. The reference Knudsen number is set up with $Kn = 0.001, 0.01$ and 0.1. With the unit Prandtl number associated with the BGK equation in Eq. (22), the coefficient of heat conductivity can be calculated via $\kappa = \mu c_p/Pr = \tau p c_p/Pr$, where c_p is the specific heat. The heat fluxes are defined by

$$\vec{q}_{Kinetic} = \frac{1}{2}\int (u - U)\left((u - U)^2 + \xi^2\right)fd\Xi, \ \ \vec{q}_{Fourier} = -\kappa\nabla T,$$

and the deviation is denoted by $\Delta q = q_{Kinetic} - q_{Fourier}$.

The computational results of convergent states at $x = 0.5$ are presented in Tables 1–3, with respect to $Kn = 0.001, 0.01$ and 0.1. The magnitude of heat flux indeed increases along with Knudsen number Kn_{ref}, which is proportional to collision time $\tau \propto Kn$, and the corresponding heat conductivity coefficient κ. The deviation between $q_{Kinetic}$ and $q_{Fourier}$ versus external force is presented in Fig. 9. It is obvious that with the increasing (decreasing) of the external force, the heat flux is enhanced (inhabited) along the direction of force. At near-equilibrium regime with relatively weak external force, the heat flux modification seems to be proportional to the magnitude of the external force. This simulation result is consistent with the conclusion in Section 2. Based on the simulation results, even in the Navier-Stokes regime a force-induced heat flux is proposed,

$$\vec{q}_{force} = \frac{(K + 3)e^{-\sigma/\tau}}{4}\frac{\sigma\vec{\phi}\rho}{\lambda}, \tag{23}$$

where $K = 2$ is the internal degree of freedom, and $\vec{\phi}$ is the forcing acceleration. The evolving time σ here is defined as a physical parameter to estimate the capability for the gas particle to transport heat during its free flight, related with the specific transport phenomenon. This definition is similar to the heat conductivity coefficient κ which measures the heat transport in a macroscopic level. We can adopt the following way to evaluate the characteristic time σ, i.e.,

$$\sigma = C\tau, \tag{24}$$

where C is a constant related with specific gas, flow condition and the truncation error in the expansion given in Eq. (15) in Section 2. In the current case, we adopt the value $C = 6.6$, and the theoretical solution based on the above equation is presented in Fig. 9 as well, denoted by the solid line. It can be seen that under relatively small external force, the numerical and theoretical solutions agree with each other well. Therefore, in the absence of shear stress in one-dimensional case, the heat flux should have the external force contribution,

$$\vec{q}_{Kinetic} = \vec{q}_{Fourier} + \vec{q}_{force} + O(\tau^2), \tag{25}$$

where the $\vec{q}_{Fourier}$ is the conventional heat flux from the temperature gradient. With the increment of Knudsen number and the magnitude of the external force, the simulation solutions deviate from the theoretical ones. It is not surprising. As the Knudsen number and collision time τ increase, the modeling in Eq. (25) loses its validity, see Fig. 9. At the highly non-equilibrium case, the gas distribution function can be far away from Maxwellian. It is very hard to identify the source of the discrepancy. For example, in the cavity case below, even without the external force the heat can transport from the cold to hot regions.

3.3. Lid-driven cavity flow under external forcing field

The cavity case is more complicated than the previous one with temperature gradient and external force in Section 3.2, the moving upper surface of the cavity will induce dissipative shear structure in the system along with the vertical external force field. In this

Table 1
Static heat conduction at $x = 0.5$ with $Kn_{ref} = 0.001$.

ϕ_x	$q_x/10^{-5}$(Kinetic)	$q_x/10^{-5}$(Fourier)	$\Delta q/10^{-5}$	$\kappa/10^{-4}$	$\nabla T/10^{-2}$
−1.0	2.972591	3.897530	−0.924939	5.146952	7.572480
−0.5	4.891944	5.360283	−0.468339	5.282272	10.14770
−0.2	5.084255	5.272859	−0.188604	5.283241	9.980360
−0.1	5.158110	5.252662	−0.094552	5.277817	9.952346
−0.05	5.202174	5.249522	−0.047348	5.273871	9.953838
−0.02	5.230964	5.250001	−0.019037	5.271195	9.959797
−0.01	5.241005	5.250429	−0.009424	5.270205	9.962479
−0.005	5.246134	5.250869	−0.004735	5.269701	9.964267
−0.003	5.248152	5.251060	−0.002908	5.269498	9.965012
−0.002	5.249229	5.251114	−0.001885	5.269395	9.965310
−0.001	5.250274	5.251248	−0.000974	5.269292	9.965757
0	5.251317	5.251304	0.000013	5.269192	9.966055
0.001	5.252173	5.251324	0.000849	5.269291	9.965906
0.002	5.253001	5.251110	0.001891	5.269391	9.965310
0.003	5.253776	5.250895	0.002881	5.269490	9.964714
0.005	5.255487	5.250781	0.004706	5.269691	9.964118
0.01	5.259658	5.250244	0.009414	5.270177	9.962181
0.02	5.267780	5.248820	0.018960	5.271113	9.957711
0.05	5.291033	5.243666	0.047367	5.273672	9.943108
0.1	5.326649	5.231825	0.094824	5.276869	9.914646
0.2	5.382336	5.192234	0.190102	5.282511	9.829114
0.5	5.565373	5.087006	0.478367	5.283018	9.628990
1.0	7.600921	6.628320	0.972601	5.145493	12.88177

case, the square cavity has four walls with length $L = 1$. The upper wall moves in tangential direction (positive x–direction) with a velocity $U_w = 0.15$. A series of external forcing acceleration ϕ_y is set up in the negative y-direction. The magnitude of force ϕ_y is denoted by g. Non-dimensional Froude number can be defined in this system to quantify the relative importance of the upper wall's driven velocity and the effect of external force,

$$Fr = \frac{U_w}{\sqrt{gL}}. \qquad (26)$$

The initial density and pressure are defined with barometric balance state,

$$\rho(x, y, t = 0) = \exp(2\phi_y y), \quad p(x, y, t = 0) = \exp(\phi_y y),$$
$$U(x, y, t = 0) = 0.$$

The initial particle distribution function is set as Maxwellian everywhere with respect to stratified density in the cavity. The wall temperature is kept with $T_w = 1$, and the full Maxwell accommodation boundary condition is used in the simulation. The Prandtl number of the gas in this case is $Pr = 0.67$ with Shakhov model. The reference Knudsen number is selected as $Kn_{ref} = 0.001, 0.075, 1.0$, which is defined by reference state at bottom of the cavity $\rho_{ref} = 1.0$ and $p_{ref} = 1.0$. The dynamic viscosity in the reference state is calculated via variable hard sphere (VHS) model,

$$\mu_{ref} = \frac{5(\alpha + 1)(\alpha + 2)\sqrt{\pi}}{4\alpha(5 - 2\omega)(7 - 2\omega)} Kn_{ref}. \qquad (27)$$

Here we choose $\alpha = 1.0$ and $\omega = 0.5$ to recover a hard sphere monatomic gas in the reference state, and its viscosity model is

Table 2
Static heat conduction at $x = 0.5$ with $Kn_{ref} = 0.01$.

ϕ_x	$q_x/10^{-4}$(Kinetic)	$q_x/10^{-4}$(Fourier)	$\Delta q/10^{-4}$	$\kappa/10^{-3}$	$\nabla T/10^{-2}$
−1.0	4.159400	4.923694	−0.764294	5.285504	9.315470
−0.5	4.671721	5.109767	−0.438046	5.276438	9.684125
−0.2	4.960925	5.147284	−0.186359	5.271861	9.763697
−0.1	5.054733	5.149716	−0.094983	5.270331	9.771148
−0.05	5.101326	5.149271	−0.047945	5.269553	9.771744
−0.02	5.129215	5.148576	−0.019361	5.269082	9.771297
−0.01	5.138495	5.148263	−0.009768	5.268923	9.771000
−0.005	5.143113	5.148028	−0.004915	5.268844	9.770701
−0.003	5.144938	5.147840	−0.002902	5.268812	9.770403
−0.002	5.145862	5.147825	−0.001963	5.268797	9.770403
−0.001	5.146787	5.147810	−0.001023	5.268781	9.770403
0	5.147720	5.147716	0.000004	5.268766	9.770254
0.001	5.148651	5.147704	0.000947	5.268753	9.770254
0.002	5.149587	5.147692	0.001895	5.268740	9.770254
0.003	5.150518	5.147599	0.002919	5.268727	9.770105
0.005	5.152359	5.147494	0.004865	5.268699	9.769956
0.01	5.156859	5.147195	0.009664	5.268633	9.769509
0.02	5.166055	5.146598	0.019457	5.268504	9.768615
0.05	5.193455	5.144636	0.048819	5.268104	9.765634
0.1	5.238829	5.140213	0.098616	5.267432	9.758481
0.2	5.328186	5.127297	0.200889	5.266018	9.736577
0.5	5.585669	5.053397	0.532272	5.261136	9.605148
1.0	5.975517	4.779735	1.195782	5.247476	9.108642

Table 3
Static heat conduction at $x = 0.5$ with $Kn_{ref} = 0.1$.

ϕ_x	$q_x/10^{-3}$(Kinetic)	$q_x/10^{-3}$(Fourier)	$\Delta q/10^{-3}$	$\kappa/10^{-2}$	$\nabla T/10^{-2}$
−1.0	3.325840	3.675841	−0.349999	5.364258	6.852468
−0.5	3.806697	3.959946	−0.292500	5.333717	7.424362
−0.2	4.128662	4.317960	−0.189298	5.292371	8.158840
−0.1	4.216921	4.346055	−0.129135	5.278889	8.232900
−0.05	4.257409	4.343608	−0.086200	5.272100	8.238860
−0.02	4.280470	4.336932	−0.056461	5.267998	8.232602
−0.01	4.287953	4.333683	−0.045730	5.266625	8.228578
−0.005	4.291654	4.331940	−0.040286	5.265938	8.226343
−0.003	4.293129	4.331243	−0.038114	5.265663	8.225449
−0.002	4.293863	4.330894	−0.037031	5.265525	8.225002
−0.001	4.294597	4.330467	−0.035870	5.265387	8.224406
0	4.295335	4.330040	−0.034705	5.265249	8.223810
0.001	4.296064	4.330467	−0.033705	5.265111	8.223512
0.002	4.296792	4.329264	−0.032472	5.264974	8.222767
0.003	4.297520	4.328916	−0.031396	5.264836	8.222320
0.005	4.298975	4.328062	−0.029087	5.264560	8.221128
0.01	4.302596	4.326083	−0.023487	5.263871	8.218446
0.02	4.309760	4.321574	−0.011815	5.262488	8.212038
0.05	4.330614	4.305378	0.025236	5.258318	8.187748
0.1	4.363158	4.269412	0.093746	5.251281	8.130230
0.2	4.419476	4.162659	0.256817	5.236785	7.948883
0.5	4.504970	3.535368	0.969598	5.188042	6.814457
1.0	4.233966	1.159689	3.074266	5.073368	2.285840

(a) $Kn_{ref} = 0.001$
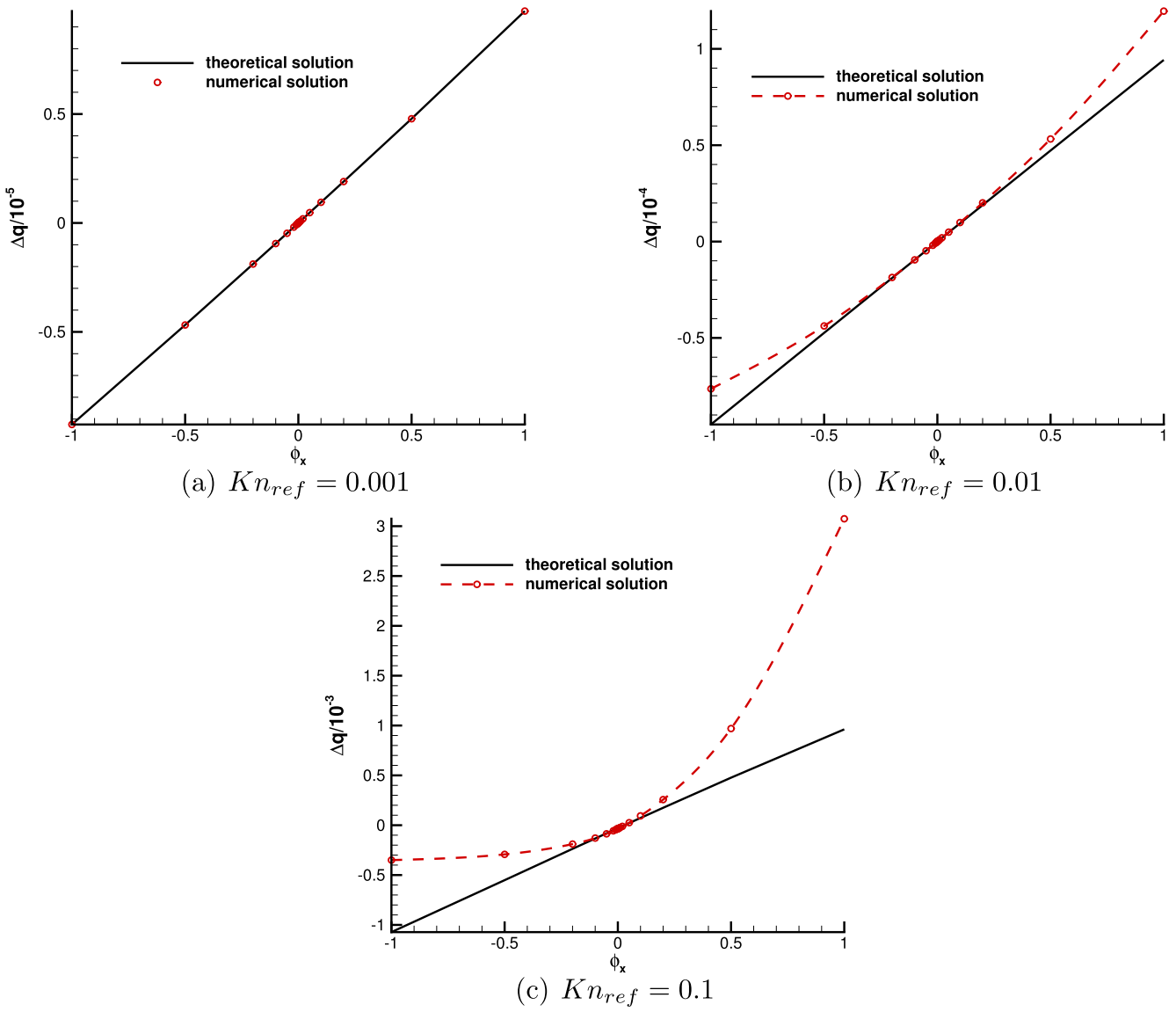
(b) $Kn_{ref} = 0.01$

(c) $Kn_{ref} = 0.1$

Fig. 9. The variation of $\Delta q = q_{UGKS} - q_{Fourier}$ versus external force ϕ_x. The red circle is computational result, the red dashed line is spline fit and the black line is analytical solution.
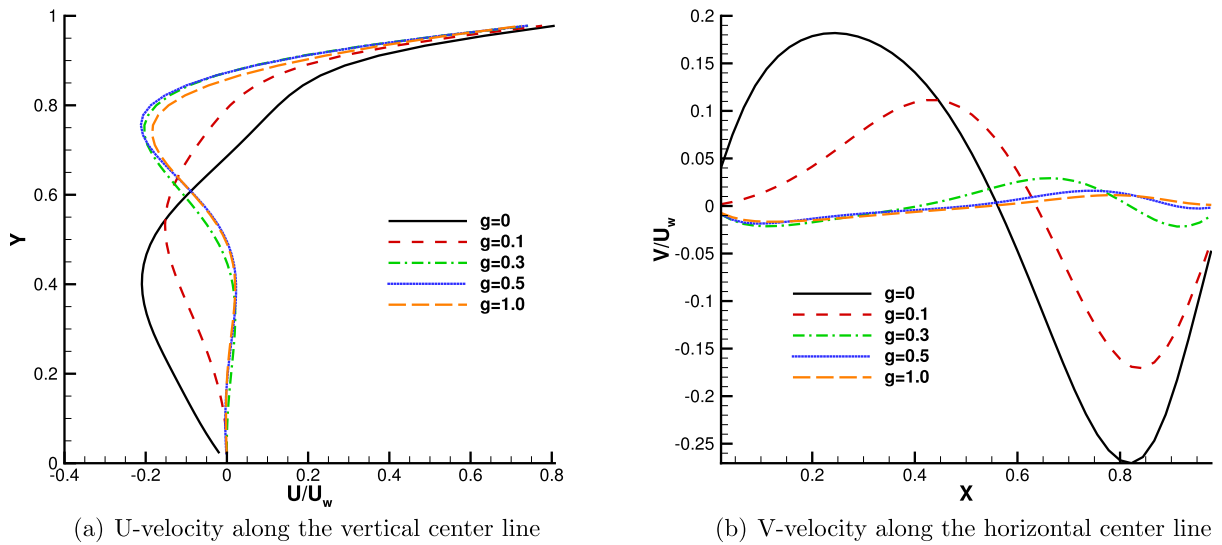

(a) U-velocity along the vertical center line

(b) V-velocity along the horizontal center line

Fig. 10. Velocity distribution along the center line with $Kn_{ref} = 0.001$.

$$\mu = \mu_{ref}\left(\frac{T}{T_{ref}}\right)^{\theta}, \tag{28}$$

where T_{ref} is the reference temperature and θ is the index related to HS model. In this case we adopt the value $\theta = 0.72$. The local collision time is evaluated with the relation $\tau = \mu/p$. The computational domain is covered by 45×45 uniform cells. The velocity space is discretized into 28×28 Gaussian points [39] at $Kn_{ref} = 0.001$, while a 89×89 non-uniform mesh [40,41] is employed for non-equilibrium flow simulation at $Kn_{ref} = 0.075$ and $Kn_{ref} = 1.0$.

3.3.1. Near equilibrium flow

For the cavity case, the movement of upper surface and the external forcing term are two sources for the fluid motion and energy transport. At $Kn_{ref} = 0.001$, the initial hydrostatic distribution under external force field is perturbed by the upper wall's
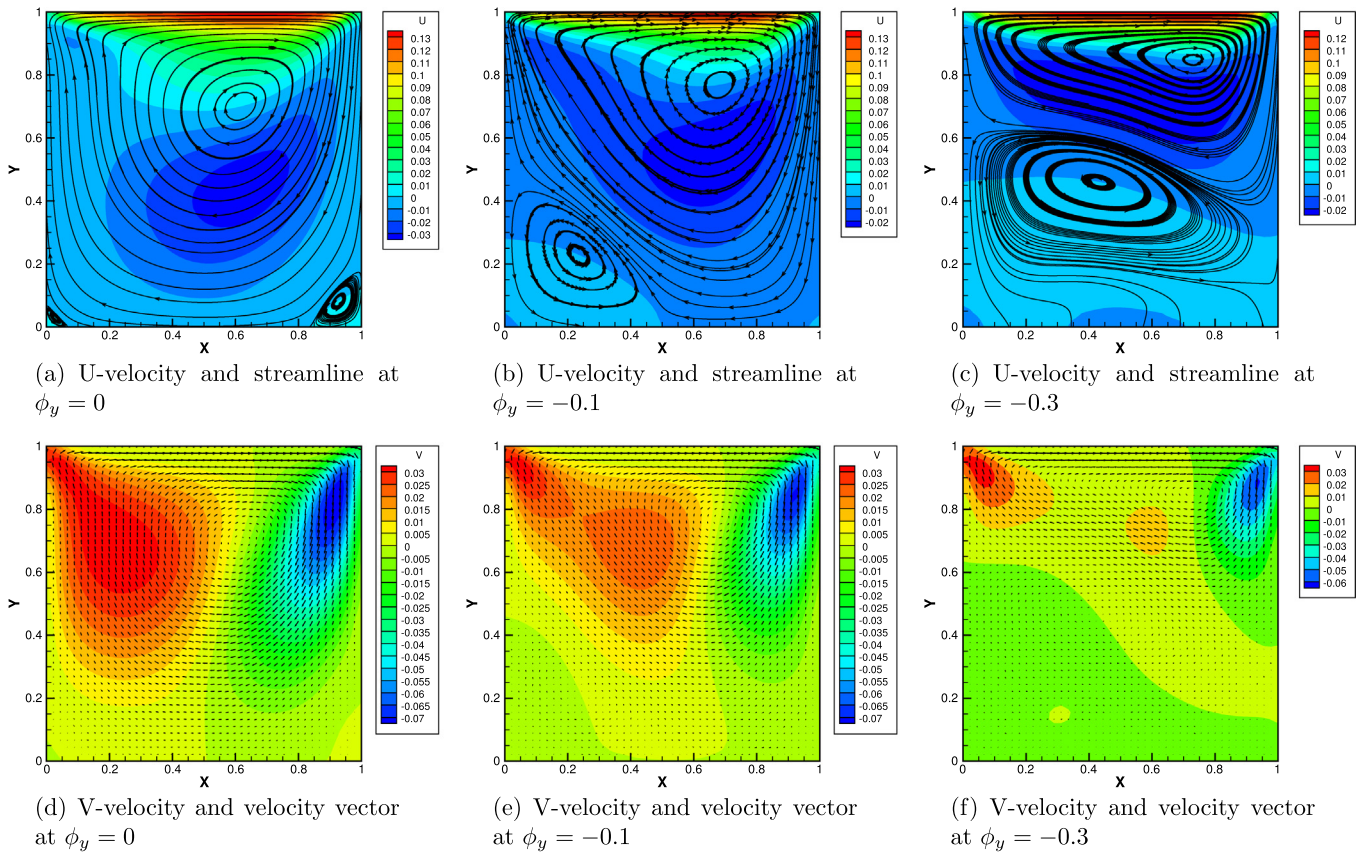

(a) U-velocity and streamline at $\phi_y = 0$

(b) U-velocity and streamline at $\phi_y = -0.1$

(c) U-velocity and streamline at $\phi_y = -0.3$

(d) V-velocity and velocity vector at $\phi_y = 0$

(e) V-velocity and velocity vector at $\phi_y = -0.1$

(f) V-velocity and velocity vector at $\phi_y = -0.3$

Fig. 11. Velocity distribution with $Kn_{ref} = 0.001$.
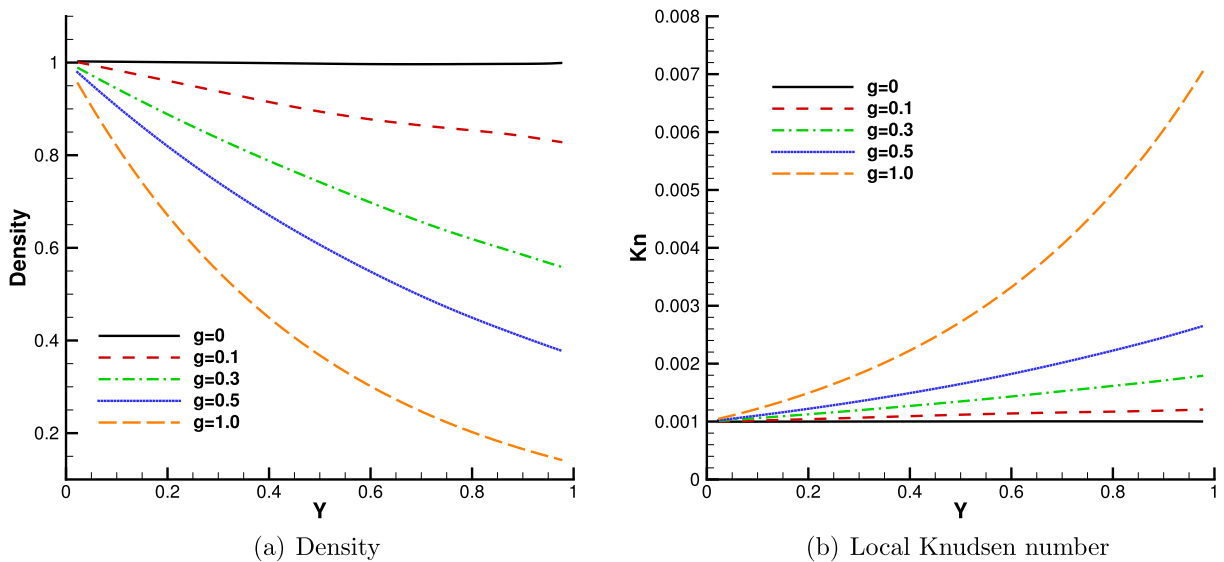

(a) Density

(b) Local Knudsen number

Fig. 12. Density and local Knudsen number distribution along the vertical center line with $Kn_{ref} = 0.001$.

sudden movement. The viscous shear triggers the flow movement inside the cavity. Due to initial large density variation, the flow pattern is much more complicated than the cases without external force, especially for the cases with a large variation of local Knudsen numbers. In the current study, the external forcing acceleration takes the values $\phi_y = 0.0, -0.1, -0.3, -0.5, -1.0$ separately in the
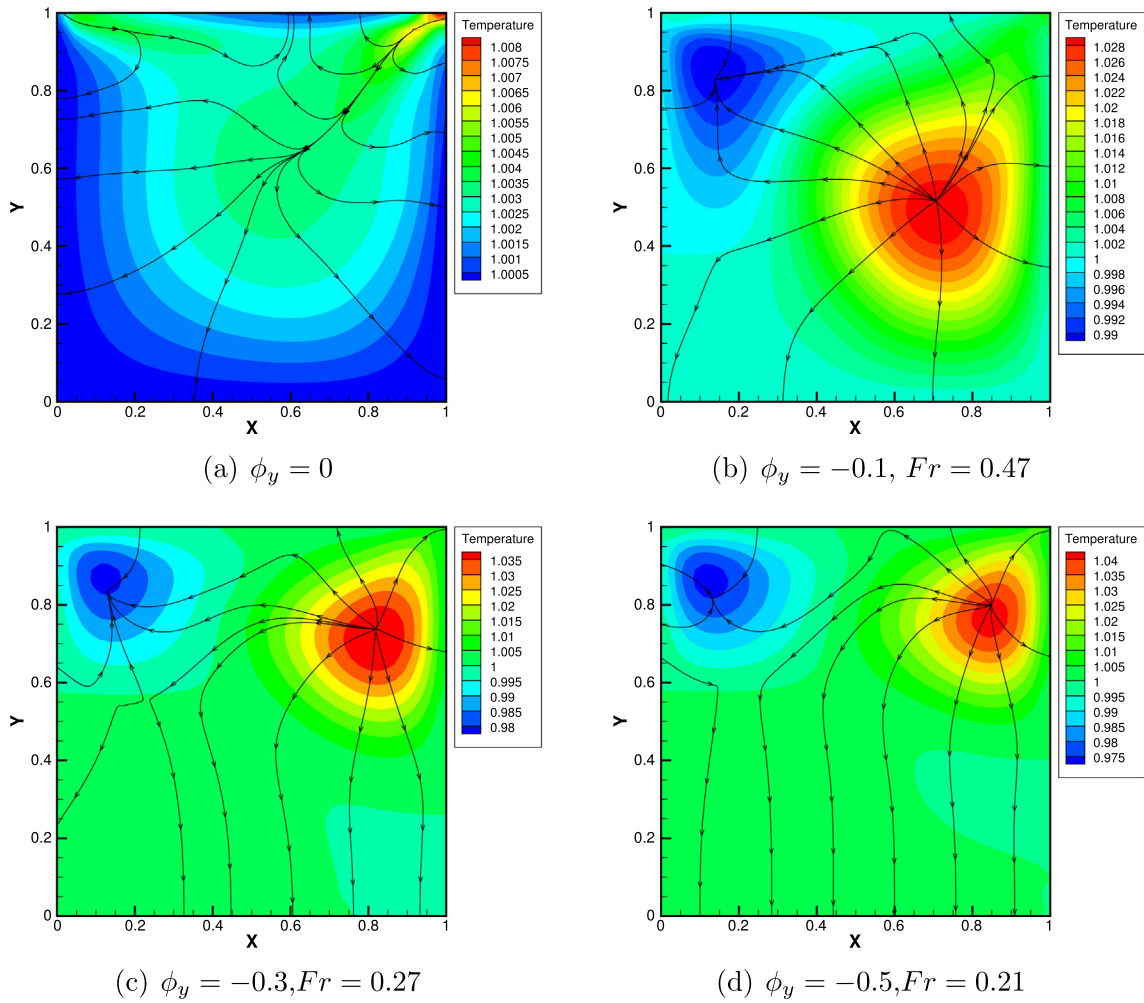

(a) $\phi_y = 0$

(b) $\phi_y = -0.1$, $Fr = 0.47$

(c) $\phi_y = -0.3, Fr = 0.27$

(d) $\phi_y = -0.5, Fr = 0.21$

Fig. 13. Temperature contour and heat flux with $Kn_{ref} = 0.001$.

(a) U-velocity along the vertical center line

(b) V-velocity along the horizontal center line

Fig. 14. Velocity distribution along the center line with $Kn_{ref} = 0.075$.

negative $y-$direction. Fig. 10 shows the velocity distribution along the center lines at $Kn_{ref} = 0.001$ in the near continuum limit. Fig. 11 presents velocity contours, vector fields, and streamlines at $\phi_y = 0, -0.1, -0.3$ inside the cavity. As shown, in the case with a small magnitude of external force, there exists a large eddy in the almost whole cavity domain with two small corner vortices, and the distribution of U-velocity along the vertical center line varies simply. However, with the increment of external force, the flow pattern changes dramatically. With a strong external force field, the eddy is confined in the upper half domain of the cavity, and the high density region in the lower part forms a weak and reversed running vortex starting from the left corner of the cavity. An inflexion point appears in the U-velocity curve and the lower part flow is almost stationary. In fact, as presented in Fig. 12a, with the relatively large external force, there is an obvious density variation along the vertical center line. As a result, the flow in the upper region of the cavity stays in the transition flow regime with an significant increment of the local Knudsen number, see Fig. 12b for the Knudsen number distributions along the central vertical line.

The heat transfer inside the cavity is closely coupled with flow transport. Fig. 13 presents the temperature contour and the heat flux under different external forcing at $Kn_{ref} = 0.001$. In the absence of external force case, particle collisions at the top right corner result in a viscous heating at the macroscopic level, see Fig. 13a. Due to intensive particle collisions, the expansion cooling at the top left corner is not obvious in this case, and the temperature around other three boundaries is almost uniform. This is consistent with the NS solution in the continuum regime [9]. With an increment of external forcing term, the localized hot and cold spots no longer stay at the corner regions, and propagate into the cavity. The penetration of the temperature spots is related to the scale of the main eddy. From the results in Figs. 13 and 10, the center of the hot spot is around the location where the negative U-velocity approaches to its maximum value, and the center of the cold spot locates a little bit higher than the hot one. At the current
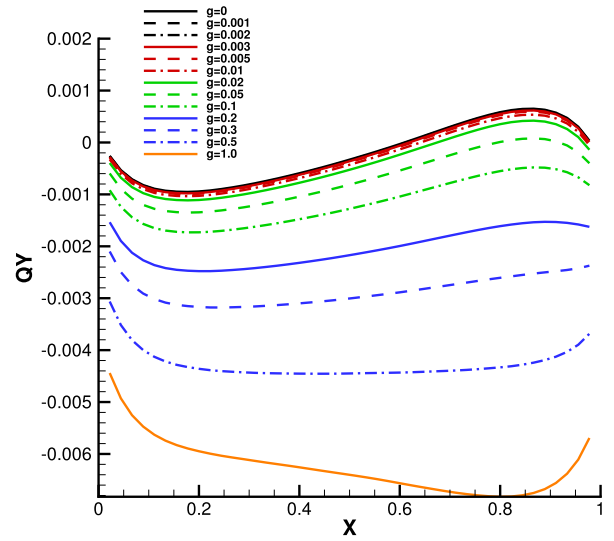

Fig. 16. Heat flux distribution along the horizontal center line with $Kn_{ref} = 0.075$.

(a) $\phi_y = 0$

(b) $\phi_y = -0.1, Fr = 0.47$

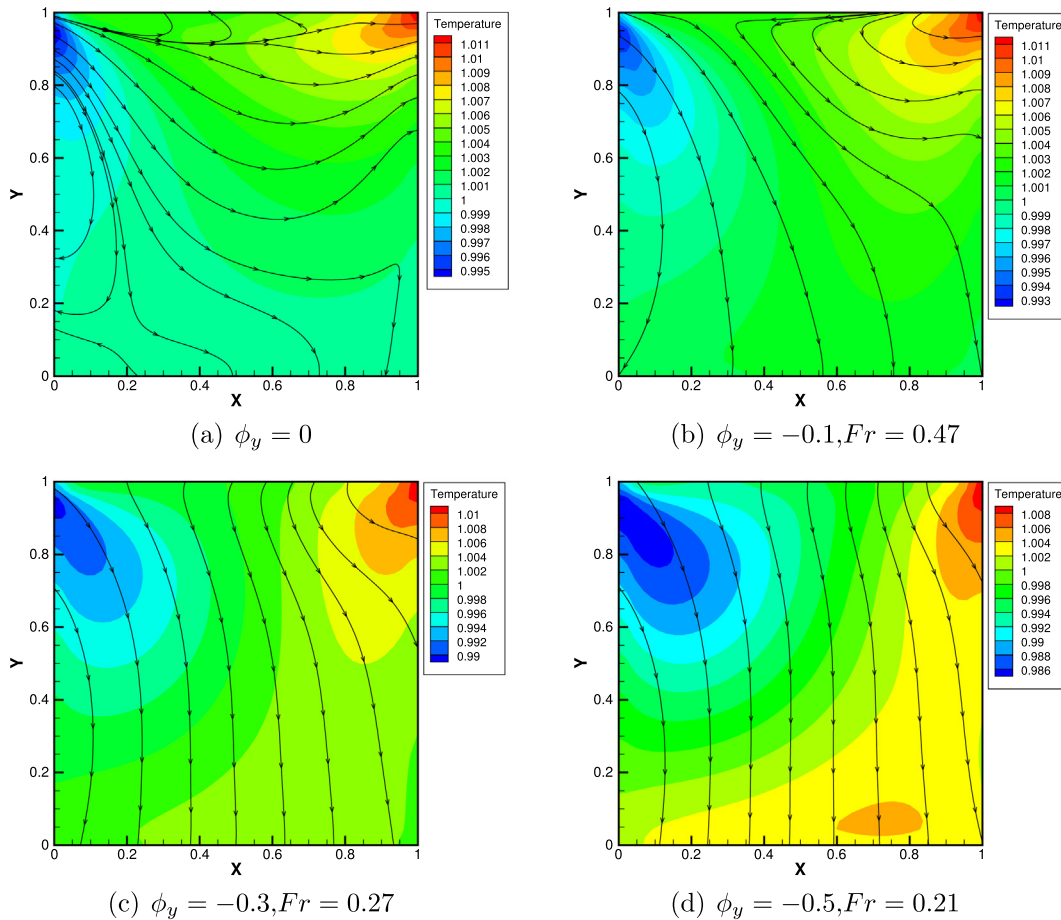(c) $\phi_y = -0.3, Fr = 0.27$

(d) $\phi_y = -0.5, Fr = 0.21$

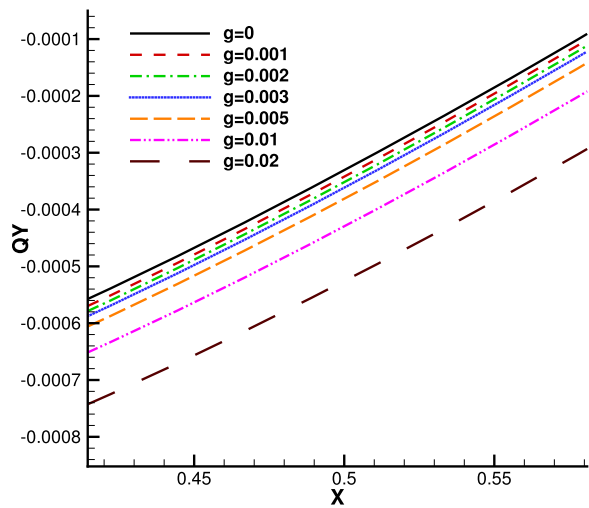Fig. 15. Temperature contour and heat flux with $Kn_{ref} = 0.075$.

$Kn_{ref} = 0.001$ case, the particle distribution function near the bottom wall will not deviate much from the Maxwellian distribution. Due to the existence of distinct inhomogeneous temperature distribution, the heat flux is mainly aligned with the temperature gradient in the upper domain. However, in the lower near-static region where there is no significant temperature difference, the heat flux shows the tendency to line up with the direction of the external force field. The adjustment of particle distribution function under external forcing provides a rich non-equilibrium heat transport mechanism besides the heat conduction from the temperature gradient.
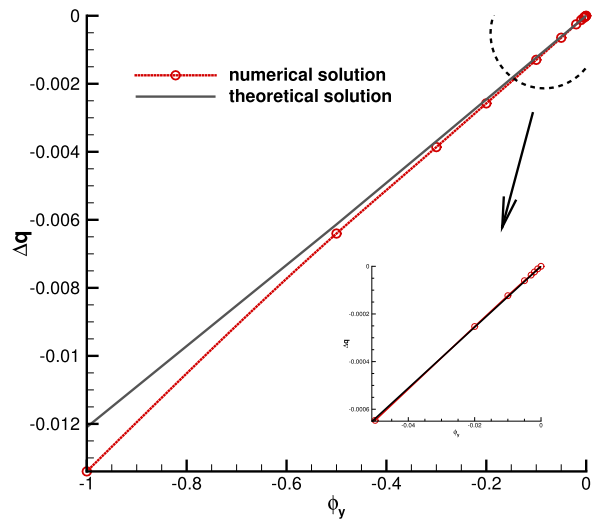
3.3.2. Non-equilibrium flow

Now let us turn our attention to the cases in the transition flow regime at $Kn_{ref} = 0.075$ and $Kn_{ref} = 1.0$. In these cases, the external forcing accelerations have the values $\phi_y = 0.0, -0.001, -0.002, -0.003, -0.005, -0.01, -0.02, -0.05, -0.1, -0.2, -0.3, -0.5, -1.0$ separately along the negative y-direction. As shown in Figs. 14 and

18, the particle penetration and efficient mixing in the transition regime generate one large eddy in all cases. The stabilizing effect due to external force field is to reduce the rotating speed of the vortex. With the increment of external force, the velocity profile is flattened, indicating a weaker vortex motion.

In the non-equilibrium cases the external force field exerts a great influence on the heat transfer process. As presented in Figs. 15 and 19, in the absence of external force field, both the expansion cooling and viscous heating have distinguishable contributions to the heat flux, where the phenomena for the heat flux from cold to hot regions is observed. This observation is consistent with the DSMC simulation and unified scheme solution [9,21]. With the increment of the external force, the heat transfer gradually turns to the vertical direction along the forcing field. As demonstrated, even with the viscous heating from the isothermal upper wall, due to the external force guided energy transport the temperature decreases there and results the cooling of the upper near wall region.
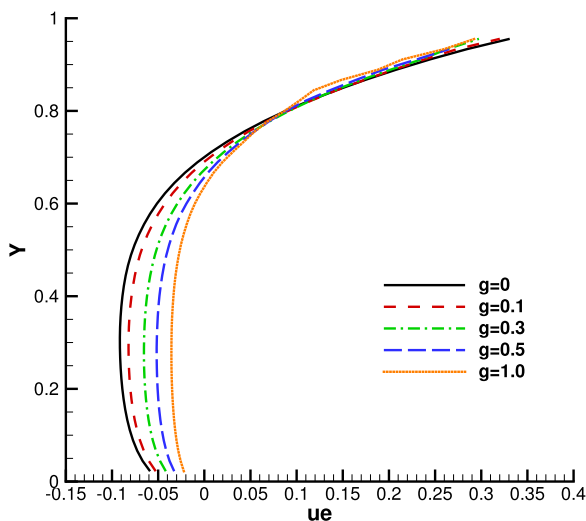

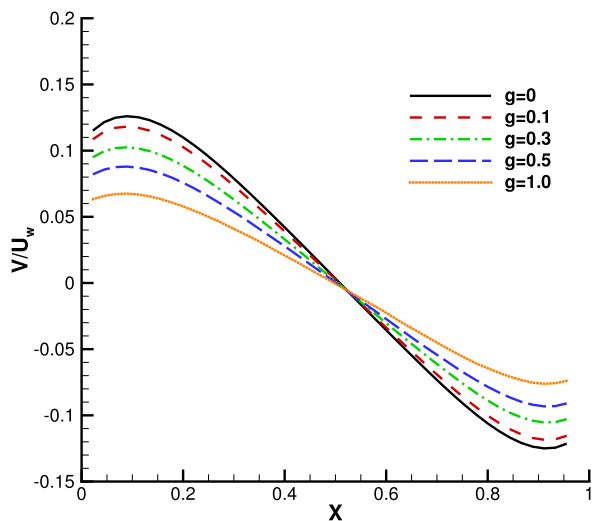(a) Horizontal distribution of q_y near the cavity center

(b) Heat flux difference $q_y - q_0$ versus the external force ϕ_x at cavity center point

Fig. 17. Heat flux distribution near the cavity center with $Kn_{ref} = 0.075$.

(a) U-velocity along the vertical center line

(b) V-velocity along the horizontal center line

Fig. 18. Velocity distribution along the center line with $Kn_{ref} = 1.0$.

Here in Fig. 16 we first present the distribution of y-direction heat flux along the horizontal center line at $Kn_{ref} = 0.075$. Since there is almost no temperature variation in the vertical direction near the center of the cavity, the heat flux there can be attributed mainly to the external force effect. It can be observed that an increment of external force enhances the magnitude of heat flux q_y in the same direction. Fig. 17a shows the horizontal distribution of q_y near the cavity center. At weak force fields, all curves are nearly parallel with each other and the intervals between them are related to the differences of the force magnitudes. In Fig. 17b, we plot the heat flux $q_y - q_0$ at the cavity center $x = y = 0.5$, where q_0 is the y-direction heat flux calculated by the Fourier's law $q_0 = -\kappa \partial T / \partial y$. The numerical results are denoted by red circles, and the red line is the spline fitting curve of discretized results. Based on the theoretical analysis in Section 2, we present in the black line as well, the theoretical force-induced heat flux based on local collision time, density and temperature, i.e., $\vec{q}_{force} = (K + 3)e^{-\sigma/\tau} \sigma \vec{\phi}_y \rho / 4\lambda$, where the internal degree of freedom $K = 1$ and the characteristic time $\sigma = 3.5\tau$. It can be seen that in the linear region where the force is relatively small, these two solutions are consistent with each other. With the increment of external force, the highly non-equilibrium dynamics deviates the force-driven heat flux from the theoretical linear relationship.

Figs. 18 and 19 show the flow velocity distributions, temperature contours, and the heat fluxes for the system under the external force field at Knudsen number 1.0. Fig. 20 presents the distribution of heat flux in y-direction along the horizontal center line. Here all the profiles of heat flux intersect with each others under different magnitude of external force acceleration. With the increment of external force, the q_y curve is flattened gradually, and finally becomes a monotonic decreasing profile along the x-direction. At Knudsen number $Kn_{ref} = 1.0$, the gas dynamics gets to highly non-equilibrium. For example, in the case with $\phi_y = -0.5$, the heat flux is almost parallel to the external force direction at lower part of the cavity, and the heat transport is in
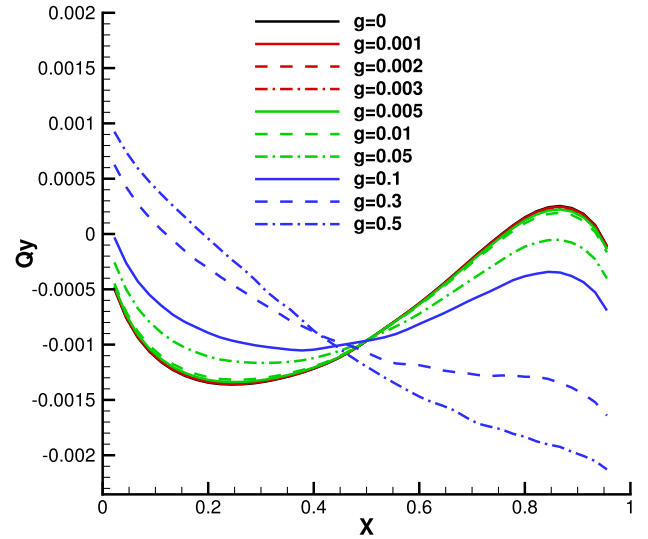

Fig. 20. Heat flux distribution along the horizontal center line with $Kn_{ref} = 1.0$.

(a) $\phi_y = 0$

(b) $\phi_y = -0.1, Fr = 0.47$

(c) $\phi_y = -0.3, Fr = 0.27$

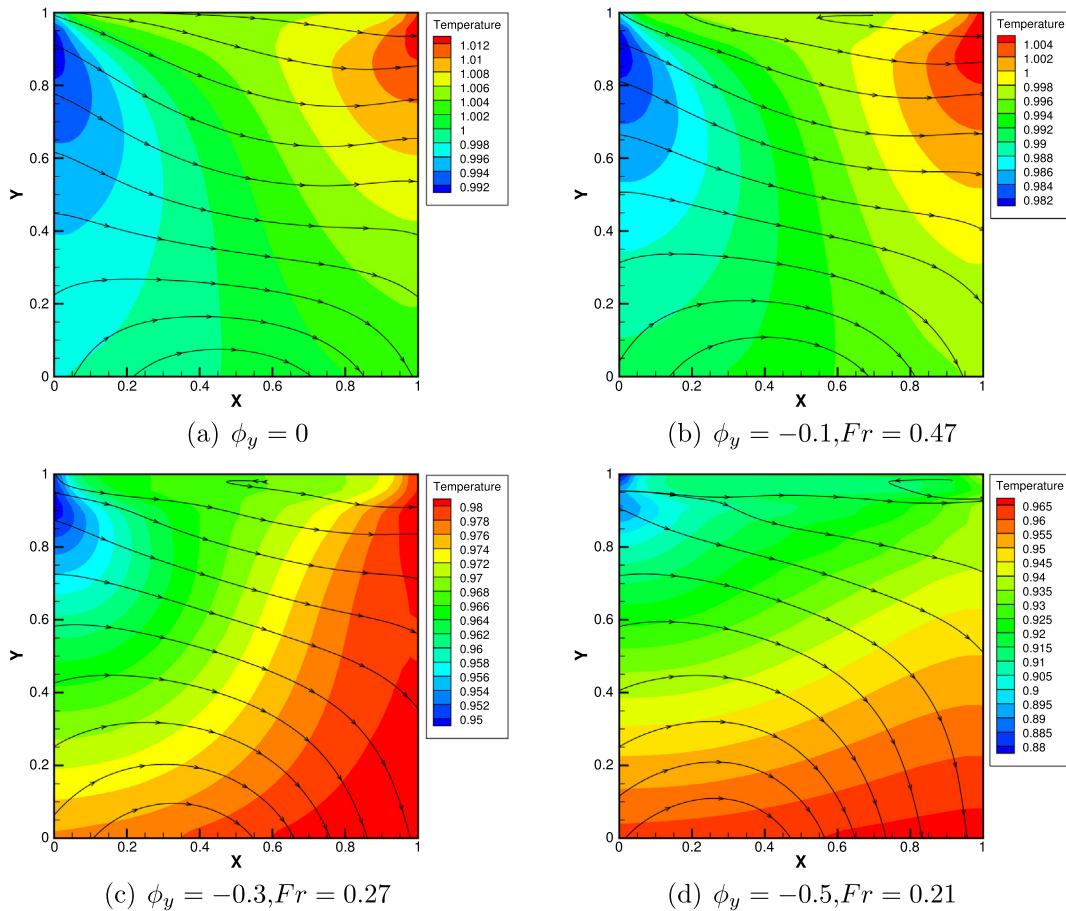(d) $\phi_y = -0.5, Fr = 0.21$

Fig. 19. Temperature contour and heat flux with $Kn_{ref} = 1.0$.

a non-Fourier form from the upper cold region to the bottom hot region. This phenomenon is consistent with the possible gravity-thermal instability for the thermal energy concentration to the central core region for a gravitational system. In the non-equilibrium regime, the temperature gradient, stress tensor, and external force contribute to the gas evolution in a highly nonlinear way which is beyond the linear theory given in Section 2. Fortunately, the UGKS is a reliable experimental tool to capture such a complicated physical phenomenon.

4. Conclusion

The gas dynamics under external force field is intrinsically a multiple scale flow problem due to large density variation and local Knudsen number. In this paper, based on the multiscale UGKS we investigate the heat transport in non-equilibrium flow under external force field in different regimes. The UGKS is direct modeling method on the mesh size scale. With the variation of the ratio between the mesh size and local particle mean free path, the scheme is able to present accurate cross-scale flow simulation from the Boltzmann to the Navier-Stokes solutions. For the near equilibrium flow, the additional heat flux along the forcing direction has been quantitatively evaluated through the analytical kinetic equation and the numerical simulation. At the same time, a detailed investigation for lid-driven cavity case has been conducted and the non-equilibrium flow evolution under external force field has been systematically investigated. The dynamic effect of the external force on the flow pattern and heat transfer in all flow regimes is presented. Based on the numerical experiments, the relationship between force-induced heat flux and the external force acceleration, i.e., $\overrightarrow{q}_{force} \propto \overrightarrow{\phi}$, has been quantitatively evaluated in all flow regimes. It can be used as a supplement to construct more complete energy transport in the Navier-Stokes equations. In the rarefied regime, the enhanced heat transport from the forcing term may easily overtake the contribution from the thermal diffusion. This force-driven heat flux can be used to explain the heat transport from the upper cold high-gravitational-potential region to the lower hot low-potential region and the phenomena of gravity-thermal instability. The study of the multiscale non-equilibrium flow phenomena under external force field will have great help to the understanding of large-scale atmosphere environment.

Conflict of interest

Authors declares that there is no conflict of interest.

Acknowledgement

Appendix A. Unified gas kinetic scheme

Based on the direct modeling on the cell size and time step, the unified gas kinetic scheme (UGKS) is a combination of modeling and computation, where the governing equations are constructed in a discretized space and evolved numerically. With the notation of cell averaged distribution function in the control volume,

$$f_{x_i,y_j,t^n,u_k,v_l} = f_{i,j,k,l}^n = \frac{1}{\Omega_{i,j}(\overrightarrow{x})\Omega_{k,l}(\overrightarrow{u})} \int_{\Omega_{i,j}} \int_{\Omega_{k,l}} f(x,y,t^n,u,v)d\overrightarrow{x}d\overrightarrow{u},$$

where $\Omega_{i,j} = (x_i, y_j)$ and $\Omega_{k,l} = (u_k, v_l)$ denote the control volume in physical and velocity space, the update of macroscopic flow variables and the particle distribution function are coupled in the following way,

$$\mathbf{W}_{i,j}^{n+1} = \mathbf{W}_{i,j}^n + \frac{1}{\Omega_{i,j}} \int_{t^n}^{t^{n+1}} \sum_r \Delta \mathbf{L}_r \cdot \mathbf{F}_r dt + \frac{1}{\Omega_{i,j}} \int_{t^n}^{t^{n+1}} \mathbf{G}_{i,j} dt, \tag{29}$$

$$f_{i,j,k,l}^{n+1} = f_{i,j,k,l}^n + \frac{1}{\Omega_{i,j}} \int_{t^n}^{t^{n+1}} \sum_r u_r \hat{f}_r(t) \Delta L_r dt + \frac{1}{\Omega_{i,j}} \int_{t^n}^{t^{n+1}} \int_{\Omega_{i,j}} Q(f) d\overrightarrow{x} dt$$
$$+ \frac{1}{\Omega_{i,j}} \int_{t^n}^{t^{n+1}} \int_{\Omega_{i,j}} G(f) d\overrightarrow{x} dt, \tag{30}$$

where $\mathbf{F}_r$ is the flux for macroscopic flow variables, f_r is the time-dependent gas distribution function at a cell interface for the microscopic particle flux, and ΔL_r is the cell interface length. The molecular internal degree of freedom ξ is omitted here for brevity. The $\mathbf{G}_{i,j}$ and $G(f)$ are the external forcing sources for the updates of macroscopic flow variables and particle distribution function, and $Q(f)$ is the collision term respectively,

$$\mathbf{G}_{i,j} = \int_{\Omega_{k,l}} \left(-\phi_x \frac{\partial}{\partial u} f_{i,j,k,l} - \phi_y \frac{\partial}{\partial v} f_{i,j,k,l} \right) \psi du dv, \tag{31}$$

$$Q(f) = \frac{f_{i,j,k,l}^+ - f_{i,j,k,l}}{\tau},$$
$$G(f) = -\phi_x \frac{\partial}{\partial u} f_{i,j,k,l} - \phi_y \frac{\partial}{\partial v} f_{i,j,k,l}. \tag{32}$$

Here $\overrightarrow{\phi} = \phi_x \overrightarrow{i} + \phi_y \overrightarrow{j}$ is the external force acceleration, f^+ is the equilibrium state, and $\tau = \mu/p$ is the particle collision time. Different kinetic model can be implemented to evaluate collision term $Q(f)$, such as the BGK, Shakhov [42], ES-BGK[43] and the full Boltzmann collision term [17,44]. In the current work, the Shakhov model is adopted.

In the numerical algorithm, the conservative flow variables are updated first in Eq. (29), and the updated macroscopic variables can be used for the construction of the equilibrium state in $Q(f)$ at t^{n+1} time step for an implicit treatment. The derivatives of particle velocity in $G(f)$ are evaluated via upwind finite difference method in the discretized velocity space.

For the unified gas kinetic modeling in a control volume framework, the time-dependent flux function is derived from the interface distribution function f, which is evaluated through an evolving solution of the Shakhov model. The cross-scale time-dependent integral solution is the key for the multiscale nature of UGKS. At the center of a cell interface $x_{i+1/2} = 0, y_j = 0$ and the beginning of a time step $t^n = 0$, the solution $f(0,0,t,u_k,v_l)$ is constructed as,

$$f(0,0,t,u_k,v_l) = \frac{1}{\tau} \int_0^t f^+(x',y',t',u_k',v_l') e^{-(t-t')/\tau} dt'$$
$$+ e^{-t/\tau} f_0(x^0, y^0, 0, u_k^0, v_l^0), \tag{33}$$

where $x' = -u_k'(t-t') - \frac{1}{2}\phi_x(t-t')^2, y' = -v_l'(t-t') - \frac{1}{2}\phi_y(t-t')^2$, $u_k' = u_k - \phi_x(t-t'), v_l' = v_l - \phi_y(t-t')$ are particle trajectories in physical and velocity space, and $(x^0, y^0, u_k^0, v_l^0) = (-(u_k - \phi_x t)t - \frac{1}{2}\phi_x t^2, -(v_l - \phi_y t)t - \frac{1}{2}\phi_y t^2, u_k - \phi_x t, v_l - \phi_y t)$ is the initial location of the particle which passes through the cell interface at time t. The time accumulating effect from the external forcing term on the time evolution of the particle distribution function is explicitly taken into consideration. The above multiscale solution plays the dominant role for the construction of the well-balanced UGKS, where the contributions from both equilibrium hydrodynamic and non-equilibrium kinetic flow physics are fully combined. With the

variation of the ratio between evolving time t (i.e., the time step in the computation) and particle collision time τ, the above interface distribution function covers the kinetic scale particle free transport to the hydrodynamic scale equilibrium state evolution. After the interface gas distribution function is determined, the corresponding flux for the macroscopic flow variables can be constructed as

$$\mathbf{F}_{i+1/2,j} = \int_{\Omega_{k,l}} u_k f(0,0,t,u_k,v_l)\psi \, du \, dv.$$

The discretized governing Eqs. (29) and (30) become a closed system for the time evolution.

References

[1] Toshiyuki Doi, Plane poiseuille flow of a rarefied gas in the presence of strong gravitation, Phys. Rev. E 83 (2) (2011) 026311.

[2] Toshiyuki Doi, Plane thermal transpiration of a rarefied gas in the presence of gravitation, Vacuum 86 (10) (2012) 541–1546.

[3] M. Tij, V. Garzó, A. Santos, On the influence of gravity on the thermal conductivity. arXiv preprint cond-mat/0002397, 2000.

[4] Carlo Cercignani, Rarefied Gas Dynamics: from Basic Concepts to Actual Calculations, vol. 21, Cambridge University Press, 2000.

[5] Eleuterio F. Toro, Riemann Solvers and Numerical Methods for Fluid Dynamics: A Practical Introduction, Springer Science & Business Media, 2013.

[6] K. Xu, Direct Modeling for Computational Fluid Dynamics: Construction and Application of Unified Gas-Kinetic Schemes, World Scientific, 2015.

[7] Kun Xu, Juan-Chen Huang, A unified gas-kinetic scheme for continuum and rarefied flows, J. Comput. Phys. 229 (20) (2010) 7747–7764.

[8] Tianbai Xiao, Qingdong Cai, Kun Xu, A well-balanced unified gas-kinetic scheme for multiscale flow transport under gravitational field, J. Comput. Phys. 332 (2017) 475–491.

[9] Chang Liu, Kun Xu, Quanhua Sun, Qingdong Cai, A unified gas-kinetic scheme for continuum and rarefied flows IV: full Boltzmann and model equations, J. Comput. Phys. 314 (2016) 305–340.

[10] P.N. Shankar, M.D. Deshpande, Fluid mechanics in the driven cavity, Annu. Rev. Fluid Mech. 32 (1) (2000) 93–136.

[11] U.K.N.G. Ghia, Kirti N. Ghia, C.T. Shin, High-Re solutions for incompressible flow using the Navier-Stokes equations and a multigrid method, J. Comput. Phys. 48 (3) (1982) 387–411.

[12] R. Schreiber, H.B. Keller, Driven cavity flows by efficient numerical techniques, J. Comput. Phys. 49 (2) (1983) 310–333.

[13] S. Pratap Vanka, Block-implicit multigrid solution of Navier-Stokes equations in primitive variables, J. Comput. Phys. 65 (1) (1986) 138–158.

[14] Shuling Hou, Qisu Zou, Shiyi Chen, Gary D. Doolen, Allen C. Cogley, Simulation of cavity flow by the lattice Boltzmann method, arXiv preprint comp-gas/9401003, 1994.

[15] Zhaoli Guo, Chang Shu, Lattice Boltzmann Method and its Applications in Engineering, World Scientific, 2013.

[16] Graeme Austin Bird, Molecular gas dynamics and the direct simulation of gas flows, 1994.

[17] Lei Wu, Craig White, Thomas J. Scanlon, Jason M. Reese, Yonghao Zhang, Deterministic numerical solutions of the Boltzmann equation using the fast spectral method, J. Comput. Phys. 250 (2013) 27–52.

[18] Lei Wu, Jason M. Reese, Yonghao Zhang, Oscillatory rarefied gas flow inside rectangular cavities, J. Fluid Mech. 748 (2014) 350–367.

[19] Stergios Naris, Dimitris Valougeorgis, The driven cavity flow over the whole range of the Knudsen number, Phys. Fluids (1994-present) 17 (9) (2005) 097106.

[20] Simon Mizzi, David R. Emerson, Stefan K. Stefanov, Robert W. Barber, Jason M. Reese, Effects of rarefaction on cavity flow in the slip regime, J. Comput. Theor. Nanosci. 4 (4) (2007) 817–822.

[21] Benzi John, Xiao-Jun Gu, David R. Emerson, Investigation of heat and mass transfer in a lid-driven cavity under nonequilibrium flow conditions, Numer. Heat Transf. Part B: Fundam. 58 (5) (2010) 287–303.

[22] Carlo Cercignani, The Boltzmann Equation and its Applications, Springer, 1988.

[23] L.D. Landau, E.M. Lifshitz, Fluid Mechanics, Elsevier Science, 1987.

[24] Prabhu Lal Bhatnagar, Eugene P. Gross, Max Krook, A model for collision processes in gases. I. Small amplitude processes in charged and neutral one-component systems, Phys. Rev. 94 (3) (1954) 511.

[25] Taku Ohwada, Kun Xu, The kinetic scheme for the full-burnett equations, J. Comput. Phys. 201 (1) (2004) 315–332.

[26] Walter Guido Vincenti, Charles H. Kruger, Introduction to physical gas dynamics, in: Walter Guido Vincenti, Charles H. Kruger, Introduction to Physical Gas Dynamics, vol. 1, Wiley, New York, 1965.

[27] Sydney Chapman, Thomas George Cowling, The Mathematical Theory of Non-uniform Gases: An Account of the Kinetic Theory of Viscosity, Thermal Conduction and Diffusion in Gases, Cambridge University Press, 1970.

[28] Jun Luo, Kun Xu, Na Liu, A well-balanced symplecticity-preserving gas-kinetic scheme for hydrodynamic equations under gravitational field, SIAM J. Sci. Comput. 33 (5) (2011) 2356–2381.

[29] Kun Xu, A gas-kinetic BGK scheme for the Navier–Stokes equations and its connection with artificial dissipation and Godunov method, J. Comput. Phys. 171 (1) (2001) 289–335.

[30] R. Esposito, Joel L. Lebowitz, R. Marra, Hydrodynamic limit of the stationary boltzmann equation in a slab, Commun. Math. Phys. 160 (1) (1994) 49–80.

[31] Mohamed Tij, Andrés Santos, Perturbation analysis of a stationary nonequilibrium flow generated by an external force, J. Stat. Phys. 76 (5) (1994) 1399–1414.

[32] M. Malek Mansour, Florence Baras, Alejandro L. Garcia, On the validity of hydrodynamics in plane poiseuille flows, Physica A 240 (1) (1997) 255–267.

[33] Kazuo Aoki, Shigeru Takata, Toshiyuki Nakanishi, Poiseuille-type flow of a rarefied gas between two parallel plates driven by a uniform external force, Phys. Rev. E 65 (2) (2002) 026315.

[34] Kun Xu, Super-Burnett solutions for Poiseuille flow, Phys. Fluids 15 (7) (2003) 2077–2080.

[35] F.J. Uribe, Alejandro L. Garcia, Burnett description for plane Poiseuille flow, Phys. Rev. E 60 (4) (1999) 4063.

[36] Siegfried Hess, M. Malek Mansour, Temperature profile of a dilute gas undergoing a plane Poiseuille flow, Physica A 272 (3) (1999) 481–496.

[37] Yoshio Sone, Kazuo Aoki, Hiroshi Sugimoto, The Bénard problem for a rarefied gas: formation of steady flow patterns and stability of array of rolls, Phys. Fluids (1994-present) 9 (12) (1997) 3898–3914.

[38] S. Stefanov, V. Roussinov, C. Cercignani, Rayleigh–Bénard flow of a rarefied gas and its attractors. I. Convection regime, Phys. Fluids (1994-present) 14 (7) (2002) 2255–2269.

[39] B. Shizgal, A Gaussian quadrature procedure for use in the solution of the Boltzmann equation and related problems, J. Comput. Phys. 41 (2) (1981) 309–328.

[40] Lei Wu, Jason M. Reese, Yonghao Zhang, Solving the Boltzmann equation deterministically by the fast spectral method: application to gas microflows, J. Fluid Mech. 746 (2014) 53–84.

[41] Wei Su, Scott Lindsay, Haihu Liu, Lei Wu, et al., Comparative study of the discrete velocity and lattice Boltzmann methods for rarefied gas flows through irregular channels, Phys. Rev. E 96 (2) (2017) 023309.

[42] E.M. Shakhov, Generalization of the Krook kinetic relaxation equation, Fluid Dyn. 3 (5) (1968) 95–96.

[43] Lowell H. Holway Jr., New statistical models for kinetic theory: methods of construction, Phys. Fluids (1958–1988) 9 (9) (1966) 1658–1673.

[44] Lei Wu, Jun Zhang, Jason M. Reese, Yonghao Zhang, A fast spectral method for the Boltzmann equation for monatomic gas mixtures, J. Comput. Phys. 298 (2015) 602–621.